

Dynamics of phenyl-based polymer chains confined in thin layers

BACHELOR THESIS

for the attainment of the academic degree

Bachelor of Science

at the

International Physics Study Program (IPSP) of the University of Leipzig

submitted by

Federico Porcelli

born on 16.03.2001 in Bisceglie

prepared in the
IPSP Leipzig

Supervised by

Dr. Martin Treß, Prof. Dr. Frank Cichos

Decision on the conferral of the bachelor degree dated 15.09.2024

Contents

| | |
|---|-----------|
| Bibliography | i |
| List of Abbreviations | ii |
| 1 Introduction | 1 |
| 2 Theoretical Background | 3 |
| 2.1 Basic Concepts | 3 |
| 2.1.1 Maxwell's Equations | 3 |
| 2.1.2 Electric Displacement Field | 4 |
| 2.1.3 Capacitance | 4 |
| 2.1.4 Complex Dielectric Function | 4 |
| 2.1.5 Dielectric Relaxation | 4 |
| 2.2 Modeling Functions | 5 |
| 2.2.1 Expanding on the Debye Model | 5 |
| 2.2.2 The Havriliak-Negami Function | 6 |
| 2.3 The Derivative Method | 6 |
| 2.3.1 Fitting Function for the BDS Data | 7 |
| 2.4 Relaxation in Polymers and Glass Transition | 7 |
| 2.4.1 α -Relaxation | 7 |
| 2.4.2 β -Relaxation | 8 |
| 2.5 Thin Films | 8 |
| 2.5.1 Introduction to Thin Films and the Debate about T_g Changes | 8 |
| 2.5.2 Dynamics in Thin Films | 8 |
| 2.5.3 Deconvolution and Gradient of Relaxation Time in Thin Films | 9 |
| 3 Methods & Materials | 11 |
| 3.1 Discussed Polymers | 11 |
| 3.1.1 Poly-TPD | 11 |
| 3.1.2 Poly-Bisphenol | 12 |
| 3.2 Preparation of the samples | 12 |
| 3.2.1 Solution Preparation | 12 |
| 3.2.2 Preparation of the Substrate | 13 |
| 3.2.3 Spin-Coating of the Solution | 13 |
| 3.2.4 Heating and Annealing | 14 |
| 3.3 Atomic Force Microscopy | 14 |
| 3.4 Dielectric Spectroscopy | 14 |

| | |
|--|-----------|
| 4 Results & Discussion | 17 |
| 4.1 Obtained Dielectric Spectra | 17 |
| 4.1.1 Qualitative Observations | 17 |
| 4.2 Fitting of the Data | 18 |
| 4.3 Discussion about the Obtained Parameters | 18 |
| 4.3.1 Relaxation Times | 18 |
| 4.3.2 α and β -Relaxation and Dielectric strengths $\Delta\epsilon$ | 20 |
| 4.4 Revisiting the Glass Transition Temperature Debate | 21 |
| 5 Conclusion | 23 |
| A AFM Data | 31 |
| B BDS Data | 37 |
| C Fits of BDS Data | 41 |
| D VFT/Arrhenius Fits | 59 |

Bibliography

Federico Porcelli

Dynamics of phenyl-based polymer chains confined in thin layers

Universität Leipzig, Bachelor Thesis

63 pages, 78 figures, 1 attachments

List of Abbreviations

| | |
|-----------------------|--|
| AFM | atomic force microscopy |
| BDS | broadband dielectric spectroscopy |
| DF | dielectric function |
| DSC | differential scanning calorimetry |
| ECNLE | Elastically Collective Nonlinear Langevin Equation |
| EP | electrode polarization |
| FA | fluorene |
| GPC | gel permeation chromatography |
| HN | Havriliak-Negami |
| HTL | hole transport layer |
| KK | Kramers-Kronig |
| OLED | organic light-emitting diode |
| OPV | organic photovoltaic |
| PALS | positron annihilation lifetime spectroscopy |
| Poly-Bisphenol | 4,4-Dihydroxydiphenyl-2,2-propane carbonate polymer |
| Poly-TPD | Poly([N,N'-diphenyl-N,N'-bis(4-tert-butylphenyl)-(1,1'-biphenyl)-4,4'-diamine]-alt-formaldehyde) |
| RFOT | Random First-Order Transition |
| RMS | root mean square |
| TPD | triarylamine |
| VFT | Vogel-Fulcher-Tamann |
| T_g | glass transition temperature |

Chapter 1

Introduction

Polymers are large, complex molecules made up of repeating monomer units, and they are suitable for a wide range of applications due to their versatile physical and chemical properties. Found in everyday materials such as plastics, rubber, and textiles, as well as in advanced technologies like organic electronics and biomedical devices, polymers play a critical role in modern life. Their unique characteristics, such as flexibility, strength, and durability, make them essential for a variety of industrial and technological uses [2].

In bulk form, polymers exhibit well-defined and uniform physical properties, including heat capacity, thermal expansion coefficient, dielectric permittivity, and refractive index. The glass transition temperature (T_g), an important parameter in polymer science, marks the temperature at which a polymer transitions from a glassy, rigid state to a more flexible, rubbery state. In bulk polymers, the study of T_g typically involves measuring changes in these properties as a function of temperature or time, providing a clear understanding of the materials behavior [9].

However, when polymers are confined to thin films, their behavior changes significantly due to the influence of the films boundaries and the restricted geometry. Thin films, with thicknesses ranging from nanometers to micrometers, display unique properties that are not present in bulk materials. The dynamics near the interfaces in thin films are particularly affected, leading to variations in dielectric permittivity, thermal expansion, heat capacity, and refractive index [12].

The investigation of thin polymer films has revealed that their properties are not uniform but rather exhibit a heterogeneous response due to the complex interplay of localized variations within the film. Properties like relaxation time and the use of layer models have been employed to probe the changes occurring at the interfaces. These models help in understanding how the dynamics of the polymer chains differ near the interface compared to the bulk material [10]. Studies have also shown that relaxation times behave differently near the interface, in a gradient-like fashion, with the penetration depth of these changes being a critical factor, and modelable by advanced techniques like deconvolution [2].

Typically, studies on thin polymer films have focused on flexible (i.e., with short segments) polymers, where the effects of interface-induced changes dissipate quickly as one moves away from the boundary. This leads to a relatively shallow penetration depth of these effects, limiting the resolution of measurements at the interface. However, the present work takes a different approach by focusing on stiff polymers, specifically Poly-TPD and P-Bisphenol, where the size of segments is higher. The aim is to utilize the greater chain stiffness of these polymers to achieve a deeper penetration of the interface effects, thereby indirectly enhancing the resolution of the measurements and providing a more detailed understanding of the dynamics at play [2].

By employing broadband dielectric spectroscopy (BDS), this work seeks to provide a com-

hensive data set that can be used to better understand the interface effects in thin films. The stiffer polymer chains are expected to exhibit more pronounced and longer-lasting interface-induced effects, allowing for a clearer resolution of the gradients in relaxation times across the film. This data will be valuable for deconvolution analyses, which aim to separate the different contributions to the overall dielectric response of the film and offer insights into how these effects influence the glass transition temperature in confined geometries, which is a topic still debated in research.

Therefore, this work aims to shed light on the unique behaviors of stiff polymer thin films and contribute to the ongoing debate about how confinement influences the glass transition temperature. By providing detailed data on the dielectric response and relaxation processes in these films, it is hoped to advance the understanding of polymer dynamics under confinement and offer a more refined model of how these materials behave in thin film form.

Chapter 2

Theoretical Background

2.1 Basic Concepts

This section introduces the foundational concepts necessary to grasp the subject matter, drawing upon the framework as discussed by Kremer [6].

2.1.1 Maxwell's Equations

Maxwell's equations form the basics of classical electromagnetism, describing how electric charges and currents produce electric and magnetic fields, as well as how those fields interact with each other and with matter. It is deemed worthwhile to quickly recall them [11]:

Gauß Theorem for Electricity:

$$\nabla \cdot \mathbf{E} = \frac{\rho}{\epsilon_0} \quad (2.1)$$

Gauß Theorem for Magnetism:

$$\nabla \cdot \mathbf{B} = 0 \quad (2.2)$$

Faraday's Law of Induction:

$$\nabla \times \mathbf{E} = -\frac{\partial \mathbf{B}}{\partial t} \quad (2.3)$$

Ampère's Law (with Maxwell's addition):

$$\nabla \times \mathbf{B} = \mu_0 \mathbf{J} + \mu_0 \epsilon_0 \frac{\partial \mathbf{E}}{\partial t} \quad (2.4)$$

Here, $\nabla \cdot$ denotes divergence, $\nabla \times$ denotes curl, \mathbf{E} is the electric field, \mathbf{B} is the magnetic field, ρ is the charge density, \mathbf{J} is the current density, ϵ_0 is the permittivity of free space, and μ_0 is the permeability of free space.

2.1.2 Electric Displacement Field

The electric displacement field \mathbf{D} relates to the electric field \mathbf{E} and the polarization \mathbf{P} within a medium. It accounts for both free and bound charges in the material and is defined by the equation:

$$\mathbf{D} = \epsilon_0 \mathbf{E} + \mathbf{P} = \epsilon_0 \epsilon \mathbf{E}$$

where \mathbf{P} is the polarization vector (i.e. dipole moment per unit volume of the material), and ϵ represents the dielectric function (DF) and is generally a tensor of rank 2 because of the non-required collinearity between \mathbf{D} and \mathbf{E} [4].

2.1.3 Capacitance

Capacitance C is the ability of a system to store electric charge per unit voltage, defined as $C = \frac{Q}{V}$. For a parallel-plate capacitor, consisting of two conductive plates separated by a dielectric, the capacitance is given by:

$$C = \frac{\epsilon_0 \epsilon_r A}{d} \quad (2.5)$$

where ϵ_r is the relative permittivity of the dielectric material, A is the area of the plates, and d is the distance between them.

2.1.4 Complex Dielectric Function

In most instances though, ϵ is treated as a complex (scalar) function $\epsilon^*(\omega)$, which varies with frequency due to the contributions of different oscillators in the analyzed materials. Namely it is given by:

$$\epsilon^* = \epsilon' + i\epsilon''$$

where the complex ϵ'' and the real ϵ' parts are related by the Kramers-Kronig relation [1].

2.1.5 Dielectric Relaxation

The dielectric relaxation theory for small electric field strengths is a specific application of linear response theory, applicable to isotropic systems. In this context, the time-dependent response $y(t)$ of a system, following a disturbance $x(t)$, is described by a linear equation. For dielectrics, the disturbance is the time-dependent external electric field $x(t) = E(t)$, and the response is the polarization $y(t) = P(t)$. This relationship is given by [6]:

$$P(t) = P_\infty + \epsilon_0 \int_{-\infty}^t \epsilon(t-t') \frac{dE(t')}{dt'} dt'$$

where $\epsilon(t)$ is the time-dependent dielectric function, and P_∞ includes all contributions from induced polarization. This equation relies on the principles of linearity (the system's response to multiple disturbances is the sum of individual responses) and causality (only past disturbances influence the response at time t).

When a stationary periodic electric field $E(t) = E_0 e^{-i\omega t}$ is applied, the equation transforms to:

$$P(t, \omega) = \epsilon_0 (\epsilon^*(\omega) - 1) E(t, \omega)$$

The relationship between the time-dependent dielectric function $\epsilon(t)$ and the complex dielectric function $\epsilon^*(\omega)$ is given by:

$$\epsilon^*(\omega) = \epsilon_\infty - \int_0^\infty \frac{d\epsilon(t)}{dt} e^{-i\omega t} dt \quad (2.6)$$

This expression is a one-sided Fourier or full imaginary Laplace transformation, which in conjunction with the relaxation time approximation, as seen in the following section, will lead to the arising of the Debye model of dielectric relaxation, upon which further models are based.

2.2 Modeling Functions

When analyzing dielectric spectra, it all comes down to give physical models that give insight into the occurring phenomena. A simple, commonly-used approximation is the model of relaxation time. The most general way to understand it is that the time derivative of a quantity is proportional to the quantity itself [4]. As an instance:

$$\frac{dP(t)}{dt} = -\frac{P(t)}{\tau_D}$$

where τ_D is the characteristic relaxation time. Solving this equation yields an exponential decay for the correlation function $\Phi(\tau)$:

$$\Phi(\tau) = \exp\left(-\frac{\tau}{\tau_D}\right)$$

Using this approximation together with Equation 2.6 leads to the following complex dielectric function $\epsilon^*(\omega)$ [6]:

$$\epsilon^*(\omega) = \epsilon_\infty + \frac{\Delta\epsilon}{1 + i\omega\tau_D} \quad (2.7)$$

where $\Delta\epsilon = \epsilon_S - \epsilon_\infty$ is the dielectric relaxation intensity, with $\epsilon_S = \lim_{\omega \rightarrow 0} \epsilon'(\omega)$ and $\epsilon_\infty = \lim_{\omega \rightarrow \infty} \epsilon'(\omega)$.

The Debye relaxation time τ_D is related to the position of maximal loss by

$$\omega_p = \frac{2\pi}{\nu_p} = \frac{1}{\tau_D} \quad (2.8)$$

Equation 2.7 is known as Debye relaxation, and is the basis for further models that will be discussed next.

2.2.1 Expanding on the Debye Model

The Debye model above is, however, not sufficient to describe all the effects that happen within the dielectric spectra in most cases. Therefore, non-Debye models have been introduced, and a short outline will be discussed below.

A commonly used model is the Cole-Cole function, given by [6]:

$$\epsilon_{CC}^*(\omega) = \epsilon_\infty + \frac{\Delta\epsilon}{1 + (i\omega\tau_{CC})^\beta}$$

where $0 < \beta \leq 1$. This function introduces a symmetrical broadening of the relaxation function, with the Debye function recovered when $\beta = 1$. The characteristic relaxation time τ_{CC} determines the position of maximal loss, defined analogously as in Equation 2.8.

For cases where the dielectric function exhibits asymmetric broadening, the Fuoss-Kirkwood or Cole-Davidson functions are more appropriate. The Cole-Davidson function is expressed as [6]:

$$\epsilon_{\text{CD}}^*(\omega) = \epsilon_\infty + \frac{\Delta\epsilon}{(1 + i\omega\tau_{\text{CD}})^\gamma}$$

Here, $0 < \gamma \leq 1$ introduces asymmetry, with the Debye function being a special case when $\gamma = 1$. The characteristic relaxation time τ_{CD} does not necessarily correspond to the position of maximal loss, which is instead given by:

$$\omega_p = \frac{1}{\tau_{\text{CD}}} \tan\left(\frac{\pi}{2\gamma + 2}\right)$$

2.2.2 The Havriliak-Negami Function

A more general approach is provided by the Havriliak-Negami (HN) function, which combines features of both the Cole-Cole and Cole-Davidson functions [6]:

$$\epsilon_{\text{HN}}^*(\omega) = \epsilon_\infty + \frac{\Delta\epsilon}{(1 + (i\omega\tau_{\text{HN}})^\beta)^\gamma}$$

In the HN function, $0 < \beta, \gamma \leq 1$, where β and γ describe the symmetric and asymmetric broadening, respectively. The behavior of the dielectric function at low and high frequencies, $\epsilon_s - \epsilon'(\omega) \sim \omega^m$ and $\epsilon'' \sim \omega^m$ for $\omega \ll 1/\tau_{\text{HN}}$, is characterized by the exponent $m = \beta$.

The dielectric function's behavior at high frequencies can be described by the following relationships:

$$\epsilon'(\omega) - \epsilon_\infty \sim \omega^{-n} \quad \text{and} \quad \epsilon'' \sim \omega^{-n} \quad \text{for} \quad \omega \gg \frac{1}{\tau_{\text{HN}}}$$

with $n = \beta\gamma$. The parameters m and n , introduced by Jonscher, represent the slopes of $\log \epsilon''$ versus $\log \omega$ at low and high frequencies, respectively, relative to the position of maximal loss.

The position of maximal loss ω_p depends on the shape parameters β and γ as follows:

$$\omega_p = \frac{1}{\tau_{\text{HN}}} \left[\sin\left(\frac{\beta\pi}{2+2\gamma}\right) \right]^{\frac{1}{\beta}} \left[\sin\left(\frac{\beta\gamma\pi}{2+2\gamma}\right) \right]^{-\frac{1}{\beta}}$$

and therefore,

$$\tau_c(\beta, \gamma) = \tau_{\text{HN}} \left[\sin\left(\frac{\pi\beta\gamma}{2+2\gamma}\right) \right]^{-\frac{1}{\beta}} \left[\sin\left(\frac{\pi\beta}{2+2\gamma}\right) \right]^{\frac{1}{\beta}}$$

corresponds to the relaxation time at maximum loss peak [12].

2.3 The Derivative Method

Due to the significant conductivity contribution, which obscures the clear observation of the loss peak near the glass transition temperature, the derivative method has to be employed [13]. This consists in exploiting the Kramers-Kronig (KK) relation to one's advantage: since the integral transform of ϵ' doesn't include the (ionic) Ohmic conduction term, it will contain the same information as ϵ'' without this conductivity contribution.

An easy way to interpret ϵ' is to take its derivative and using the relationship:

$$\epsilon''_{\text{der}} = \left(-\frac{\pi}{2}\right) \frac{d\epsilon'}{d \ln f} \approx \epsilon''_{\text{rel}}$$

which means that the HN function for the derivative of ϵ' will have the form:

$$\frac{\partial \epsilon'_{\text{HN}}}{\partial \ln f} = -\frac{\beta \gamma \Delta \epsilon \cdot (2\pi f \tau)^{\beta} \cos[\beta \frac{\pi}{2} - (1+\gamma)\theta_{\text{HN}}]}{\left[1 + 2(2\pi f \tau)^{\beta} \cos\left(\frac{\beta\pi}{2}\right) + (2\pi f \tau)^{2\beta}\right]^{(1+\gamma)/2}}$$

where

$$\theta_{\text{HN}} = \arctan\left[\frac{\sin(\pi\beta/2)}{(2\pi f \tau)^{-\beta} + \cos(\pi\beta/2)}\right]$$

and the rest of the parameters are defined as before.

2.3.1 Fitting Function for the BDS Data

Based on these considerations, the fitting function for the data will have the following form:

$$F(\Delta\epsilon_i, \tau_{\text{HN}_i}, \beta_i, \gamma_i, \sigma_0, a) = \sum_{i=1}^3 \left(\frac{\partial \epsilon'_{\text{HN}}}{\partial \ln f} \right)_i + \frac{\sigma_0}{\epsilon_0 \omega^a} \quad (2.9)$$

where the first term consists in multiple HN functions which are summed together – up to three, depending on the number of peaks in the spectrum – and the second term indicates the electrode polarization (EP), which usually happens at low frequencies before the first HN peak, and has the form of a DC conductivity, but is not always occurring and thus optional.

2.4 Relaxation in Polymers and Glass Transition

Relaxation processes in polymers are fundamental to understanding their mechanical and electrical behaviors – especially in response to external stimuli such as stress or electric fields [LI2021101431]. These processes describe the return of polymer chains or segments to equilibrium after being disturbed. The relaxation behavior of polymers is highly dependent on temperature and frequency, leading to distinct relaxation modes.

The two main relaxation processes, based on the time scales and the types of molecular motions involved, are α and β -relaxations.

2.4.1 α -Relaxation

The α -relaxation is linked to large-scale, cooperative motions of polymer chains and is directly associated with the glass transition temperature (T_g) in bulk polymers. This relaxation process occurs near or above T_g , where the polymer transitions from a rigid, glassy state to a more flexible, rubbery state.

The VFT Function

The Vogel-Fulcher-Tamann (VFT) equation is a widely used empirical formula that describes the temperature dependence of the α -relaxation time in polymers. It is given by [7]:

$$\log_{10} \tau_\alpha = \log_{10} \tau_\infty - \frac{D_T T_0}{T - T_0} \quad (2.10)$$

where τ_α is the relaxation time, T is the temperature, τ_∞ is the relaxation time at infinite temperature, D_T is a material-specific constant (often referred to as the fragility parameter), and T_0 is the Vogel temperature, which is typically below the T_g .

2.4.2 β -Relaxation

The β -Relaxation is a secondary relaxation process that occurs at temperatures below T_g . It involves localized motions of smaller segments or side groups of the polymer chains, rather than the entire chain. Beta relaxations are typically observed at lower temperatures and are responsible for smaller, more subtle changes in the material's properties compared to alpha relaxation.

The Arrhenius Equation

The β -Relaxation is often noticeable by the Arrhenius behavior when plotting the beta-relaxation time versus temperature. This behavior is described by the Arrhenius Equation [15]:

$$\tau_\beta = \tau_\infty \exp\left(\frac{E}{k_B T}\right) \quad (2.11)$$

where E is the activation energy required for the relaxation process to occur, and k_B is the Boltzmann constant.

2.5 Thin Films

2.5.1 Introduction to Thin Films and the Debate about T_g Changes

Thin films, (i.e. layers of material from nanometers to micrometers thick), are important for the most disparate applications, and thus the subject of many scientific studies. A prominent topic of discussion in the study of thin films is the glass transition temperature T_g . There is an ongoing debate about whether T_g is altered in thin films compared to bulk materials [10]. This debate arises from numerous studies using techniques such as ellipsometry, neutron and X-ray reflectivity, positron annihilation lifetime spectroscopy (PALS), and thermal probe measurements. Studies have reported both increases and decreases in T_g , which hints that the interaction between the polymer and its boundaries can significantly affect its thermal properties. For instance, freely standing films of high molecular weight polystyrene have been studied, with some theories proposing that additional relaxation modes, such as a "sliding motion" of polymer chains near free surfaces, may be responsible for these observed variations [3]. This topic remains under active investigation, with theoretical models and computer simulations continuing to explore the underlying mechanisms affecting the glass transition in thin films [6].

2.5.2 Dynamics in Thin Films

The dynamics of polymers in thin films can differ significantly from those in the bulk due to a variety of factors, including chain stiffness, film thickness, and interactions at the interface [LI2021101431]. In thin films, especially those with thicknesses on the order of a few nanometers, the confinement effects and proximity to interfaces can lead to much altered molecular dynamics.

Chain stiffness plays a major role in this: while the dynamics in bulk is largely governed by the intrinsic flexibility or stiffness of the polymer chains, thin films have a reduced dimensionality that can lead to restricted chain mobility, particularly for stiffer polymers. The constraints imposed by

the film's boundaries can limit the degree of conformational changes that the polymer chains can undergo, thereby modifying the relaxation processes and overall dynamics.

Another important effect that is accentuated in thin films are interface interactions, because the surface-to-volume ratio is higher, making the influence of the substrate or surrounding medium significant. For polymers with long chain segments, the interface can induce orientation or ordering effects, which are not typically present in the bulk material.

This can lead to the emergence of new relaxation modes or the suppression of bulk relaxation processes. For instance, the sliding motion of polymer chains along their contour, proposed for freely standing films of polystyrene, is an example of how thin film dynamics can introduce mechanisms not observed in bulk polymers [12].

2.5.3 Deconvolution and Gradient of Relaxation Time in Thin Films

Relaxation time in thin films exhibits a spatial gradient, related to how molecular relaxation processes penetrate into the material from the interface.

A way to analyze this behaviour is using deconvolution techniques, which allow for the separation of overlapping relaxation processes, providing detailed insights into the distribution of relaxation times across different regions of a polymer film. This method is particularly useful when studying thin films, where the relaxation time gradient can vary significantly from the interface into the bulk-like interior of the material.

The relaxation time typically shows a pronounced gradient – starting with values that are either much shorter or much longer than those in the bulk. It then gradually transitions towards bulk-like behavior as one moves away from the interface. Several factors influence this, like chain stiffness and the strength of interactions between the polymer chains and the interface.

Near the interface, the altered mobility of polymer chains, especially in systems with long chain segments, leads to a distinctive dynamic profile. This profile can be captured by advanced models, such as those proposed in recent studies, including the work by Cheng and colleagues [2]. Their study highlights how broadband dielectric spectroscopy (BDS) can be used to reveal the spatial gradient of relaxation times. The data obtained from these analyses provide crucial input for theoretical models, such as the Random First-Order Transition (RFOT) theory and the Elastically Collective Nonlinear Langevin Equation (ECNLE) theory, both of which try to explain the interface-induced modifications in polymer dynamics [2].

Chapter 3

Methods & Materials

3.1 Discussed Polymers

Two different polymers are analyzed in this work: Poly([N,N'-diphenyl-N,N'-bis(4-tert-butylphenyl)-(1,1'-biphenyl)-4,4'-diamine]-alt-formaldehyde) (Poly-TPD) and 4,4-Dihydroxydiphenyl-2,2-propane carbonate polymer (Poly-Bisphenol).

3.1.1 Poly-TPD

Poly-TPD is from the supplier Polymer Source, Inc.TM with the sample number P16210-PolyTPD-FA, has a $M_n = 28.500$, and $M_w = 32.000$ (data from the manufacturer). It consists of triarylamine (TPD) with fluorene (FA) units incorporated into its backbone (chemical structure in Figure 3.1).

This polymer contains an FA conjugated backbone that is critical for its semiconducting properties. In particular its high hole mobility, in the range of 10^{-4} to $10^{-3} \text{ cm}^2/\text{Vs}$, makes it suitable for use as a hole transport layer (HTL) in organic light-emitting diode (OLED) and organic photovoltaic (OPV) devices.

As for its thermodynamic properties, Poly-TPD exhibits good thermal stability, with a decomposition temperature $T_d > 623\text{K}$, and a glass transition temperature around 363-423K [5].

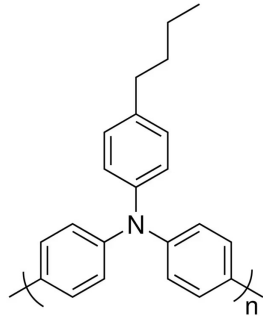


Figure 3.1: Chemical structure of Poly-TPD

3.1.2 Poly-Bisphenol

Poly-Bisphenol, on the other hand, came from the manufacturer Sigma-Aldrich[®], with the sample code 181625-250G Poly(Bisphenol A carbonate), and has a $M_w \approx 45.000$ by gel permeation chromatography (GPC), as measured by the manufacturer. Its glass transition temperature is $T_g \approx 423\text{K}$, and melting point $T_m \approx 540\text{K}$ [14]. It has the repeating unit (or monomer) as shown in Figure 3.2 and is a thermoplastic polymer with optical clarity, high tensile strength/impact resistace, high refractive index, and it is used, for example, to prepare optical lenses or as a supporting matrix to fabricate hybrid nanofiber membranes.

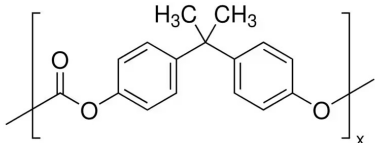


Figure 3.2: Chemical structure of Poly-Bisphenol

3.2 Preparation of the samples

The preparation of the samples required for the analysis involves creating parallel-plate capacitors on a glass substrate. These capacitors have an area of approximately $6 \times 6\text{ mm}$ and a thickness that varies from around 300 nm to 5 nm .

Controlling the thickness of the dielectric material within the capacitor is particularly important, as the goal is to study the effects of thin layers compared to the bulk material. This control is achieved by preparing polymer solutions with different concentrations: the higher the concentration, the thicker the resulting film.

3.2.1 Solution Preparation

In particular, 7 solutions were prepared for each of the polymers starting from a concentration of 20 mg/ml and roughly halved. The solvent used for Poly-TPD was Chloroform (CHCl_3 , manufacturer Sigma-Aldrich[®], sample number C2432-1L), while Poly-Bisphenol was diluted in Dichloromethane (CH_2Cl_2 , manufacturer Sigma-Aldrich[®], sample number 32222).

To determine the volume needed to dilute a solution from an initial concentration of 20 mg/ml to a desired concentration of e.g. 10 mg/ml in a final volume of 10 ml , the dilution formula can be used $C_1 V_1 = C_2 V_2$. Here, C_1 is the initial concentration (20 mg/ml), C_2 is the desired concentration (10 mg/ml), and V_2 is the final volume (10 ml). To find V_1 , the volume of the initial solution one can solve for V_1 as follows:

$$V_1 = \frac{C_2 V_2}{C_1} = \frac{10\text{ mg/ml} \times 10\text{ ml}}{20\text{ mg/ml}} = 5\text{ ml.}$$

Thus, 5 ml of the initial solution is required to achieve the desired concentration in a final volume of 10 ml .

This was done similarly for all other solutions, with decreasing concentrations, which correspondingly lead to decreasing thicknesses (Table 3.1).

Table 3.1: Concentrations and volumes of both sets of solutions (Poly-TPD and P-Bisphenol) created from the initial 20 mg/ml solution. The thicknesses in bold are from the samples that were measured in the end (i.e. that formed correctly and didn't break/short during the measurement)

| C (mg/ml) | $V_{solution}$ (ml) | $V_{solvent}$ (ml) | Poly-TPD thickness (nm) | Poly-Bisphenol thickness (nm) |
|-----------|---------------------|--------------------|-------------------------|-------------------------------|
| 20 | - | - | 200 | 320 |
| 10 | 5 | 5 | 110 | 84 |
| 3 | 3 | 7 | 60 | 43 |
| 1 | 3 | 6 | 35 | 25.5 |
| 0.5 | 4 | 4 | 24 | N.A. |
| 0.2 | 4 | 6 | N.A. | 17.5 |
| 0.1 | 5 | 5 | 8 | 14 |

3.2.2 Preparation of the Substrate

The glass substrates were prepared by cutting standard microscope slides into approximately 1×1 cm squares, followed by cleaning in an ultrasonic cleaner using ethanol and deionized water. This cleaning process ensures a contaminant-free surface for the deposition of polymer solutions. After cleaning, the substrates were dried using pressurized N_2 in a laminar flow hood to avoid dust contamination and then stored in a Petri dish.

Once the substrates were prepared, the next step was to create the first of the two plates of the capacitors. This was accomplished by depositing gaseous aluminum in approximately 5 mm wide strips across the substrate. Specifically, to produce a total of 9 capacitors, three equally spaced strips of aluminum were deposited. This was done using a complementary mask, which covered all areas of the substrate except for where the strips were intended to be, ensuring that the evaporated aluminum only adhered to the exposed glass surface (Figure ??).

The thermal evaporation process used for this deposition is relatively straightforward. It involves melting a small quantity of aluminum (in this case, taken from tiny cut wire) in a turbomolecular-pump vacuum chamber by heating a tungsten base with a high current. This results in the desired evaporation of the metal and its subsequent surface accumulation. The thickness of this accumulation can be controlled by adjusting the duration of the current applied to the tungsten base. Just a few seconds of heating produced an aluminum layer approximately 200 nm thick.

3.2.3 Spin-Coating of the Solution

Once the first of the two aluminum capacitor plates is deposited on the glass substrate, the next step is to apply the dielectric material between the plates. This is achieved by depositing the respective polymer solution onto the plate (Figure ??). The spin-coating technique is particularly useful in this case, as it ensures a uniform distribution of the solution across the glass layer.

A spin-coating program of 1 minute at 3000 rpm was used for all polymer solutions to ensure reproducibility.

Moreover, the glass slides were marked appropriately to allow for distinction of polymer and concentration at a later time.

3.2.4 Heating and Annealing

After spin-coating the solution, the samples were placed in a small glass container, which was then evacuated to remove any trapped air or moisture. The container was subsequently placed inside an oven set to 473K and maintained at this temperature for 12 hours to allow for annealing.

Annealing is useful for improving the film's uniformity and adhesion to the substrate, enhancing its mechanical properties, and promoting the removal of residual solvents. It also helps in stabilizing the polymer film by allowing the polymer chains to rearrange and settle into a more stable configuration.

After this process, aluminum was evaporated a second time in strips perpendicular to the earlier ones, completing the fabrication of the capacitors (Figure ??).

3.3 Atomic Force Microscopy

The use of atomic force microscopy (AFM) is particularly useful when measuring the thickness of the dielectric in the samples. Since dielectric measurements rely on the parallel plate capacitor formula (Equation 2.5), both A and d must be accurately determined. The former is a straightforward parameter to obtain, and in this case, it was measured using a simple optical microscope.

The measurement of the latter, however, is more challenging and cannot be obtained by the initial concentration of the spin-coated solution, as this would be overly imprecise and unreliable.

To accurately determine the thickness, AFM is employed in the following manner:

1. The surface of the sample is first scratched with a needle in a non-capacitor region (i.e., where no aluminum is present) as shown in the figure. This scratch allows for the measurement of the thickness of the deposited polymer layer.
2. The scratched area is then positioned under the AFM tip, with approximately half of the scratched region occupying the field of view and the non-scratched region occupying the other half.
3. This setup allows for the measurement of the relative height between the substrate and the polymer film, which is then analyzed using Gwyddion [8], where a simple statistical average of the two heights can be calculated (Figures 3.3a-3.3b), providing a relatively accurate thickness of the dielectric.

This process was repeated two or more times for each sample, and the resulting thicknesses were then averaged for each of the capacitors (Table 3.1).

3.4 Dielectric Spectroscopy

Once the parameters of the samples are known, the actual BDS measurements can be performed. This technique enables to obtain (among other things) the frequency and temperature-dependent complex and real parts of the DF ϵ^* , from which molecular dipole dynamics, polarization phenomena, and relaxation processes can be deduced. In this case, the frequency range was set up to be from 10^{-1} Hz to 10^6 Hz, and a temperature from about 290K to 530K.

A frequency generator takes care of the AC current input, with a root mean square (RMS) voltage $V_{RMS} = 0.1V$, while temperature is controlled using a Dewar flask containing liquid nitrogen, and resistances that are heated depending on the wanted temperature. The temperature of the sample is then measured using a platinum resistance thermometer, which allows for a very precise sensing of T (with an error of less than 1K).

Proper attention must be given to the connection between the sample and the BDS setup. This is achieved by using copper/gold terminals that are secured to the aluminum surface of the capacitor

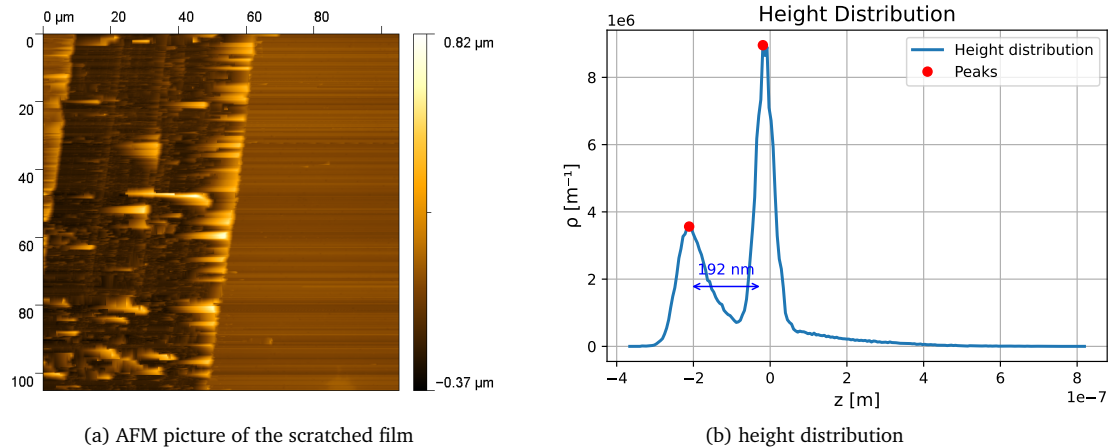


Figure 3.3: Poly-TPD thin film, sample A (200nm), example of a height distribution and AFM picture.

plates with screws, ensuring firm contact with the glass slide. Careful attention is given to ensure that the resistance is less than 2Ω across the plate and the BDS terminals, and $> 20M\Omega$ between the two plates (otherwise it would be counted as a shorted capacitor).

That done, the sample holder is placed in the setup and the measurement can be started, lasting about 18 hours for the whole temperature range to be recorded on both heating and cooling, such that reproducibility is guaranteed. However, especially in thinner films, it was noted that the sample undergoes some dielectric changes after being exposed to rapid and repeated temperature fluctuations.

Chapter 4

Results & Discussion

4.1 Obtained Dielectric Spectra

The dielectric spectra for Poly-TPD and Poly-Bisphenol were thus obtained, and the numerical derivative was then computed (as in Figure 4.1, and in Appendix B). A quick overview brings one to notice the traits discussed in the following.

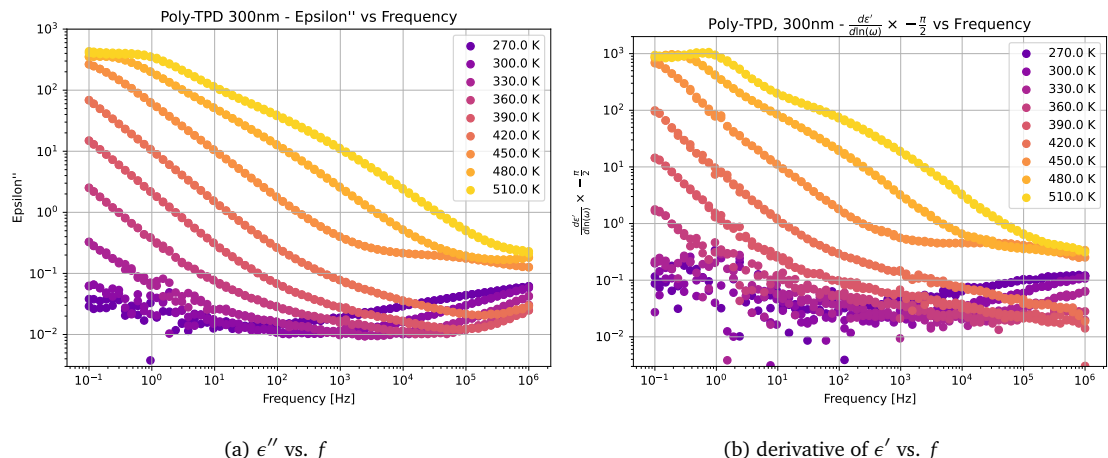


Figure 4.1: 200nm Poly-TPD thin film, complex dielectric function and derivative of the real part as a function of frequency at different temperatures (plotted once every 30 kelvin for clarity).

4.1.1 Qualitative Observations

The derivative plot is generally more helpful in identifying the occurring peaks, which are more pronounced with respect to the ϵ'' plot. This happens because of the removal of Ohmic conductivity, as discussed earlier. At low temperature, the plots become more imprecise, probably due to a combination of the electronic oscillations and computation artifacts in the case of the derivative. In some cases, a spline interpolation was used to make the data more suitable for the subsequent fitting. Thinner films generally exhibit a breakdown (i.e. shorting) at lower temperatures, although not always (as was the case of the 320nm Poly-Bisphenol film). This is consistent with the expectation that

higher temperatures facilitate the penetration of the aluminum layers in the polymer, which becomes more conductive and eventually leads to a short circuit. Also the thermal expansion of aluminum might be playing a role, though it should only be relevant for the thinner films, as its range of action is $\approx 5\text{nm}$.

4.2 Fitting of the Data

The derivative of ϵ' was then fit using Python according to Equation 2.9, for each temperature value every 10K, in a range where the data was reasonably clean (i.e. did not contain too much noise). One example of such fitted plot is shown below for the 110nm Poly-TPD (Figure 4.2, and the rest in Appendix C), where the HN1,2,3 are named from lowest frequency to highest.

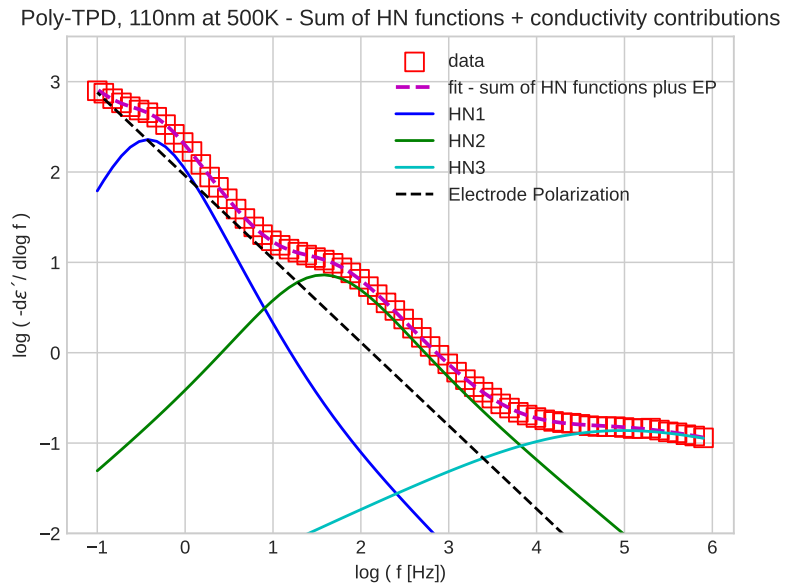


Figure 4.2: Poly-TPD 110nm thin film at 500K, fitting function

4.3 Discussion about the Obtained Parameters

4.3.1 Relaxation Times

The relaxation time τ is a parameter of interest that is drawn from the HN function fitting. The retrieved τ 's for the different polymers will now be discussed.

Poly-TPD

Three relaxation processes are visible in the spectra of this polymer, which were thus fit with three independent HN functions. It was interesting to note that these relaxation times do not always depend

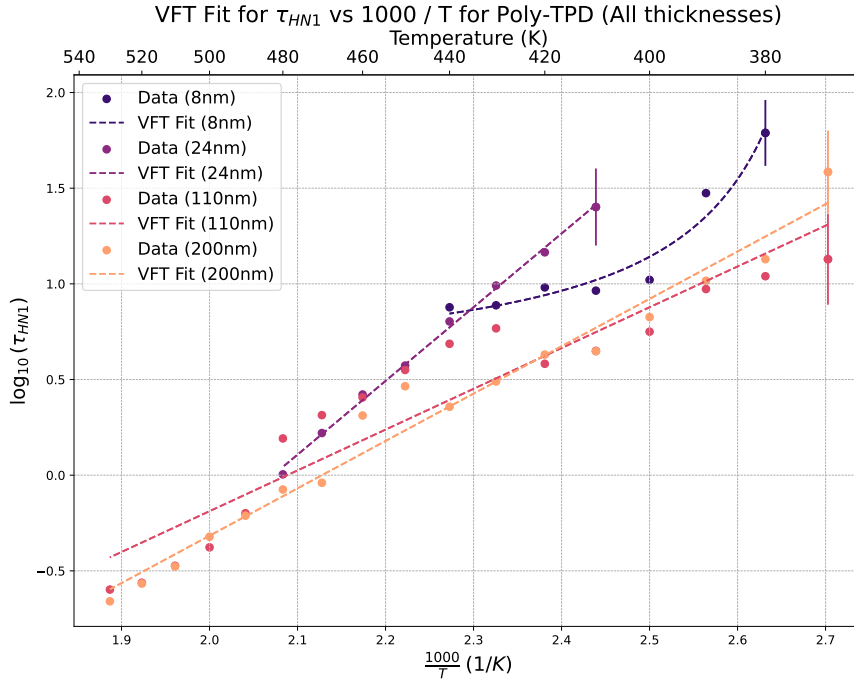


Figure 4.3: Relaxation times of the first relaxation process (i.e. obtained from the HN1 function) occurring in Poly-TPD at different thicknesses. This process seems to not depend on thickness and the different values of tau were ascribed to fitting error/noise.

on thickness. This was the case for τ_{HN1} (Figure 4.3), for which there is a coincidence (up to some noise) of the relaxation times for different thicknesses.

A different situation occurs for τ_{HN2} , which instead shows a clear thickness dependence: for low thicknesses, τ_{HN2} is much smaller than the higher counterparts. Moreover, it is reasonable to believe that a saturation may occur for very thick films (bulk), as the difference between the τ 's becomes much smaller when going from the 110nm to 200nm film, than from 8nm to 24nm (Figure 4.4).

The high frequency relaxation times modeled by the HN3 function (Figure D.2) also show a thickness dependence, but there's an overlap between the 24nm and 110nm that is not immediately explainable if not by fitting errors. Indeed, since this third peak is generally broader for all spectra, there is greater chance of the parameters being not as clearly definable as for the previous, less wide peaks.

Poly-Bisphenol

The low-frequency relaxation times (Figure D.1) look like being thickness-independent, as with Poly-TPD. In this case, the 43nm measurement was deemed inaccurate because the first peak occurs outside of the spectrum (e.g. Figure C.20b), and it's difficult to pinpoint the exact τ from just fitting. For the 14nm and 320nm, where this doesn't occur (at least at higher temperatures), the correspondence is much more apparent.

The second process (Figure 4.5) is utterly thickness dependent, and a behaviour similar as for Poly-TPD is noted: lower relaxation time for lower thickness, and vice versa. The 2nd peak for the 14nm film, as seen in ??, was very much hidden by the other peaks, and not strongly visible, which

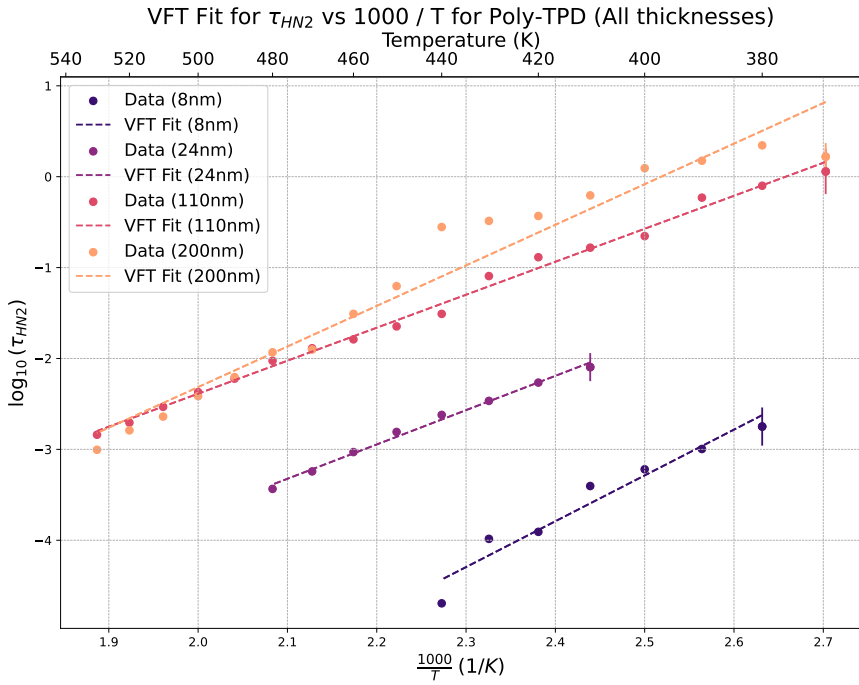


Figure 4.4: Relaxation times of the second relaxation process (i.e. obtained from the HN2 function) occurring in Poly-TPD at different thicknesses. This relaxation process suggests a thickness dependence which is discussed in the following.

is why it changes so abruptly with respect to the other ones. Still, the main difference between bulk and thin film is well-defined.

Similarly as before, the high frequency (HN3) process has a somewhat thickness-dependent relaxation time, but the relationship is again nontrivial (Figure D.3). Further experimentation is deemed necessary to better understand this behaviour.

VFT fit of the relaxation times

To interpret the relaxation times, the VFT equation is made use of, as defined in Equation 2.10. Fitting of the $\tau_{\text{HN}2}$ at different thicknesses was done for Poly-TPD (Figure 4.4) and for Poly-Bisphenol (Figure 4.5), and the parameters are represented in Tables 4.1 and 4.2, respectively. Generally speaking, an increase (in absolute value) with thickness seems to correlate all of the obtained parameters.

Of particular interest is then computing the T_g , which is defined as the temperature at which τ is equal to 10s. There is actually a debate on whether this definition is reliable or not, and some studies often define the T_g as T for $\tau = 100$ s. Nonetheless, in this work, the former definition was chosen, as the resulting T_g values resembled more closely the actual values from the manufacturer differential scanning calorimetry (DSC) experiments. Indeed,

4.3.2 α and β -Relaxation and Dielectric strengths $\Delta\epsilon$

Another useful plot for the determination of the temperature at which relaxation processes occur is fixing one frequency and plotting ϵ'' versus T . This was done for the bulk films of both polymers at

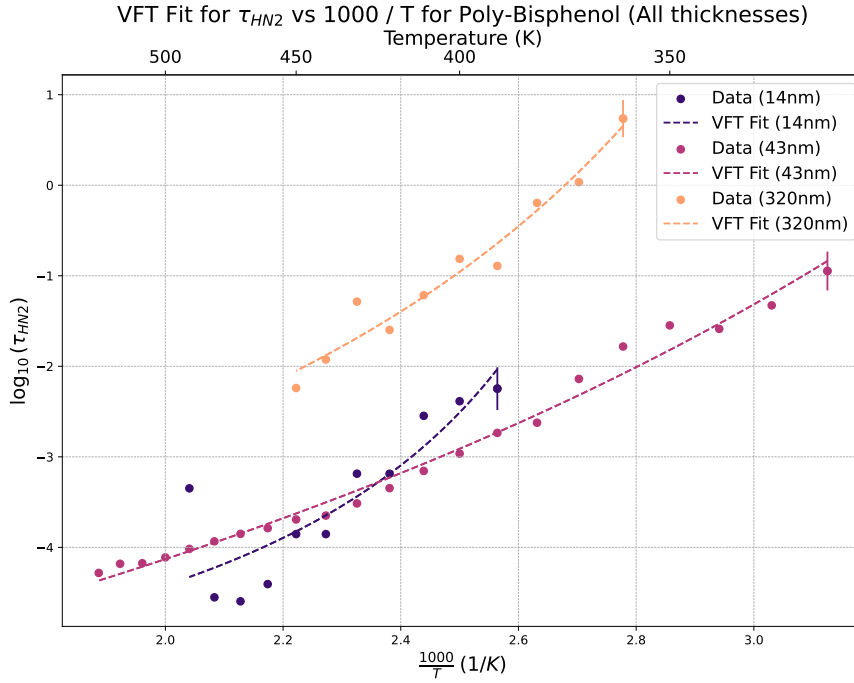


Figure 4.5: Relaxation times of the second relaxation process (i.e. obtained from the HN2 function) occurring in Poly-Bisphenol at different thicknesses. This relaxation process has a clear thickness dependence and is discussed in the following.

a frequency of about 1kHz (Figure 4.6a, Poly-TPD and Figure 4.6b, Poly-Bisphenol). As noticeable, there are no main peaks in the measured temperature range, which suggests that a greater range might be needed to show the relaxation processes. Yet, in the case of Poly-Bisphenol, a peak appears at the very edge of the spectrum, around $T=450\text{K}$, which corresponds to the α -relaxation process. This same temperature value is also confirmed in the study, and can be used as a double check for the accuracy of the gathered data.

No literature is known at the time of writing for the case of Poly-TPD, but it was considered appropriate to also show the plot, which, if anything, demonstrates that the α -relaxation occurs above 530K, and the β -relaxation below 250K.

4.4 Revisiting the Glass Transition Temperature Debate

The results from the data analysis provide an insight into the ongoing debate regarding the T_g in thin films compared to bulk materials. Specifically, these findings indicate a noticeable difference between the T_g of thin and thick films in both Poly-TPD and Poly-Bisphenol. This disparity can be attributed to the inherent stiffness of the polymer chains, which for these two polymers is particularly prominent.

Indeed, given the stiff nature of these polymers, the T_g observed in the bulk is not directly translatable to the T_g in thin films. The confined geometry of the thin films induces additional relaxation processes that are not present in the bulk material. These processes likely arise from the altered mobility and constrained dynamics of the polymer chains near the interfaces, leading to a deviation in the T_g compared to bulk samples.

Table 4.1: Fitting Parameters for Poly-TPD at different thicknesses. In this case, since $T_0 \approx 0$, the fitting reduces to Arrhenius behaviour.

| Thickness (nm) | $\log_{10}(\tau_\infty)$ | D_T | T_0 (K) | T_g (T at $\tau = 10s$ (K)) |
|----------------|--------------------------|--------------|-----------|-------------------------------|
| 8 | -15.8875 | -147223.1348 | 0.0342 | 298.47 |
| 24 | -11.2485 | -248118.7770 | 0.0152 | 308.11 |
| 110 | -9.6441 | -292768.5995 | 0.0124 | 340.89 |
| 200 | -11.2431 | -659454.5989 | 0.0068 | 364.63 |

Table 4.2: Fitting Parameters for Poly-Bisphenol at different thicknesses. The 14nm sample is likely unreliable, as discussed in the present section, and was marked in red.

| Thickness (nm) | $\log_{10}(\tau_\infty)$ | D_T | T_0 (K) | T_g (T at $\tau = 10s$ (K)) |
|----------------|--------------------------|---------|-----------|-------------------------------|
| 320 | -5.2618 | -2.4972 | 253.1543 | 354.11 |
| 43 | -7.0539 | -6.2055 | 160.1424 | 283.53 |
| 14 | -6.0000 | -0.9118 | 317.1379 | 358.45 |

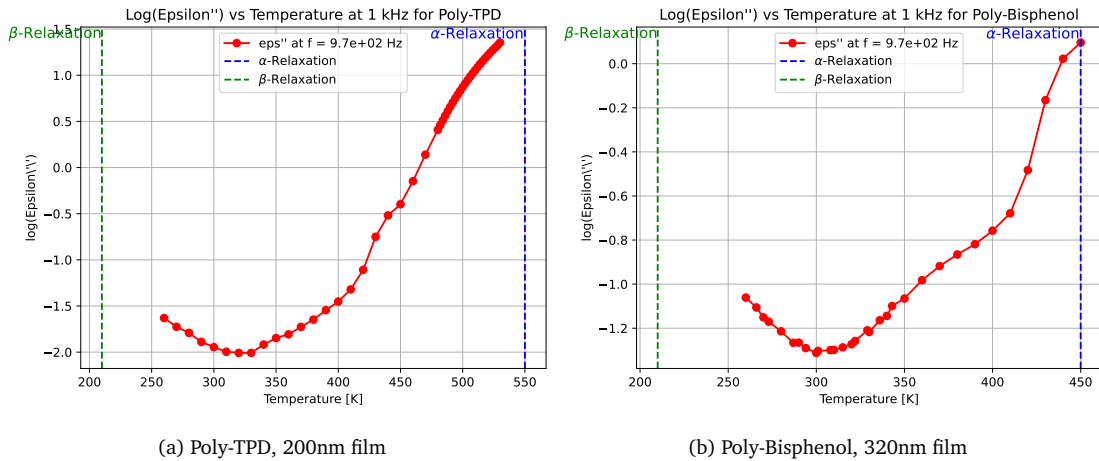


Figure 4.6: Comparison of ϵ'' vs. T for bulk Poly-TPD and Poly-Bisphenol films at $f \approx 1\text{kHz}$.

This observed difference underscores the importance of accounting for these additional relaxation mechanisms when analyzing and predicting the behavior of thin polymer films. The presence of such relaxation processes in thin films suggests that they are governed by dynamics distinct from those of the bulk, necessitating a more nuanced approach to understanding the glass transition and associated thermal properties in nanoconfined systems.

Chapter 5

Conclusion

The investigation of glass transition temperature (T_g) in thin polymer films has been a subject of considerable debate, particularly when comparing the behavior of these films to their bulk counterparts. This research delves into this debate by examining the complex dynamics of stiff polymers, specifically Poly-TPD and Poly-Bisphenol, under conditions of confinement. Through a focused analysis on how interface-induced changes affect these polymers, the present work contributes to a deeper understanding of the mechanisms governing the glass transition and relaxation processes in thin films.

Many studies on thin polymer films have predominantly focused on flexible polymers, which have short segmental lengths, like polystyrene [12]. In these polymers, the effects induced by the interface typically dissipate rapidly as one moves away from the boundary, resulting in a relatively shallow penetration depth of these effects, and thus an indifference in the T_g and other properties as the thickness of the film changes. However, the present work adopts a different approach by focusing on the stiff polymers, namely Poly-TPD and P-Bisphenol. The inherent stiffness of these polymers, characterized by longer segmental lengths, enables a deeper penetration of the interface effects into the film, thus "artificially" enhancing the resolution of these effects.

By using polymers with greater chain stiffness, this research demonstrates that the effects of confinement and interfacial interactions can penetrate more deeply into the film, providing a more detailed and nuanced understanding of the dynamics at play. The findings indicate that the T_g and relaxation processes in these stiff polymer films differ markedly from those observed in thin films of shorter-segment polymers, as well as from bulk materials, underscoring the critical role of polymer chain stiffness in determining the glass transition behavior in confined systems.

The implications of this research extend beyond the specific polymers studied, highlighting the need to consider the unique dynamics of stiff polymers in confined geometries. The deeper penetration of interface-induced effects in stiff polymers like Poly-TPD and Poly-Bisphenol offers a different perspective on the glass transition and relaxation phenomena in thin films. This understanding is crucial for optimizing the performance of polymer-based thin film technologies, particularly in applications where precise control over thermal and mechanical properties is essential.

Thesis for the attainment of the academic degree:
Bachelor of Science

Dynamics of phenyl-based polymer chains confined in thin layers

submitted by:
Federico Porcelli

prepared in:
IPSP Leipzig

supervised by:
Dr. Martin Treß, Prof. Dr. Frank Cichos

September 2024

Bibliography

- [1] H. C. Booij and G. P. J. M. Thoone. “Generalization of Kramers-Kronig transforms and some approximations of relations between viscoelastic quantities.” In: *Rheologica Acta* 21.1 (1982). Published January 1, 1982, pp. 15–24. ISSN: 1435-1528. DOI: 10.1007/BF01520701. URL: <https://doi.org/10.1007/BF01520701>.
- [2] Shiwang Cheng, David Kogut, Juncheng Zheng, Shalin Patil, Fuming Yang, and Weiyi Lu. “Dynamics of polylactic acid under ultrafine nanoconfinement: The collective interface effect and the spatial gradient.” In: *Journal of Chemical Physics* 160.11 (2024). Special Collection: Polymer Nanoconfinement, p. 114904. DOI: 10.1063/5.0189762. URL: <https://doi.org/10.1063/5.0189762>.
- [3] Ryo Fujita, Kenshiro Furudate, and Jiro Kumaki. “Atomic force microscopy of single polymer chains on a substrate at temperatures above the bulk glass transition temperatures.” In: *Polymer* 168 (2019), pp. 21–28. ISSN: 0032-3861. DOI: <https://doi.org/10.1016/j.polymer.2019.02.014>. URL: <https://www.sciencedirect.com/science/article/pii/S0032386119301351>.
- [4] Marius Grundmann. *The Physics of Semiconductors. An Introduction Including Nanophysics and Applications*. 4th ed. Graduate Texts in Physics. Springer Cham, 2021, pp. XXXVII + 889. ISBN: 978-3-030-51568-3. DOI: 10.1007/978-3-030-51569-0. URL: <https://doi.org/10.1007/978-3-030-51569-0>.
- [5] Tae-Yong Kim, Jae-Hoon Jung, Jong-Beom Kim, and Dae-Gyu Moon. “Achieving high efficiency by high temperature annealing of hole transporting polymer layer in solution-processed organic light-emitting devices.” In: *Synthetic Metals* 232 (2017), pp. 167–170. ISSN: 0379-6779. DOI: <https://doi.org/10.1016/j.synthmet.2017.08.004>. URL: <https://www.sciencedirect.com/science/article/pii/S0379677917302266>.
- [6] Friedrich Kremer and Andreas Schönhals, eds. *Broadband Dielectric Spectroscopy*. 1st ed. Springer Berlin, Heidelberg, 2003, pp. XXI, 729. ISBN: 978-3-540-43407-8. DOI: 10.1007/978-3-642-56120-7. URL: <https://doi.org/10.1007/978-3-642-56120-7>.
- [7] Rafael Levit, Julio C. Martinez-Garcia, Diego A. Ochoa, and José E. García. “The generalized Vogel-Fulcher-Tamman equation for describing the dynamics of relaxor ferroelectrics.” In: *Scientific Reports* 9.1 (Aug. 2019), p. 12390. ISSN: 2045-2322. DOI: 10.1038/s41598-019-48864-0. URL: <https://doi.org/10.1038/s41598-019-48864-0>.
- [8] David Neas and Petr Klapetek. *Gwyddion*. Version 2.56. Initial release on March 2, 2004 (preview version 0.99.1). URL: <https://gwyddion.net>.
- [9] Shogo Saito and Tatsuji Nakajima. “Glass transition in polymers.” In: *Journal of Applied Polymer Science* 2.4 (1959), pp. 93–99.

- [10] A. Serghei, M. Tress, and F. Kremer. “The glass transition of thin polymer films in relation to the interfacial dynamics.” In: *The Journal of Chemical Physics* 131.15 (Oct. 2009). Institute for Experimental Physics I, University of Leipzig, and Department of Polymer Science and Engineering, University of Massachusetts Amherst, p. 154904. DOI: 10.1063/1.3248368. URL: <https://doi.org/10.1063/1.3248368>.
- [11] Frederick Tombe. “Maxwell’s Original Equations.” In: (Dec. 2011).
- [12] Roksana Winkler, Aparna Beena Unni, Wenkang Tu, Katarzyna Chat, and Karolina Adrjanowicz. “On the Segmental Dynamics and the Glass Transition Behavior of Poly(2-vinylpyridine) in One- and Two-Dimensional Nanometric Confinement.” In: *The Journal of Physical Chemistry B* 125.23 (2021). Downloaded via 181.215.217.186 on May 29, 2021 at 18:55:43 (UTC). See <https://pubs.acs.org/sharingguidelines> for options on how to legitimately share published articles., pp. 6298–6310. DOI: 10.1021/acs.jpcb.1c01245. URL: <https://doi.org/10.1021/acs.jpcb.1c01245>.
- [13] Michael Wübbenhorst and Jan van Turnhout. “Analysis of complex dielectric spectra. I. One-dimensional derivative techniques and three-dimensional modelling.” In: *Journal of Non-Crystalline Solids* 305 (2002). Department of Polymer Materials & Engineering, Delft University of Technology, pp. 40–49. URL: <https://www.elsevier.com/locate/jnoncrysol>.
- [14] Huajie Yin, Simone Napolitano, and Andreas Schönhals. “Molecular Mobility and Glass Transition of Thin Films of Poly(bisphenol A carbonate).” In: *Macromolecules* 45 (2012). Received: September 20, 2011; Revised: January 12, 2012; Published: January 30, 2012, pp. 1652–1662. DOI: 10.1021/ma202127p. URL: <https://dx.doi.org/10.1021/ma202127p>.
- [15] Ding Zhao, Baohua Yue, et al. “On the viscosity of molten salts and molten salt mixtures and its temperature dependence.” In: *Journal of Energy Storage* (2023). Article discusses the temperature dependence of the viscosity of molten salts using the Arrhenius equation.

Declaration of Independent Work

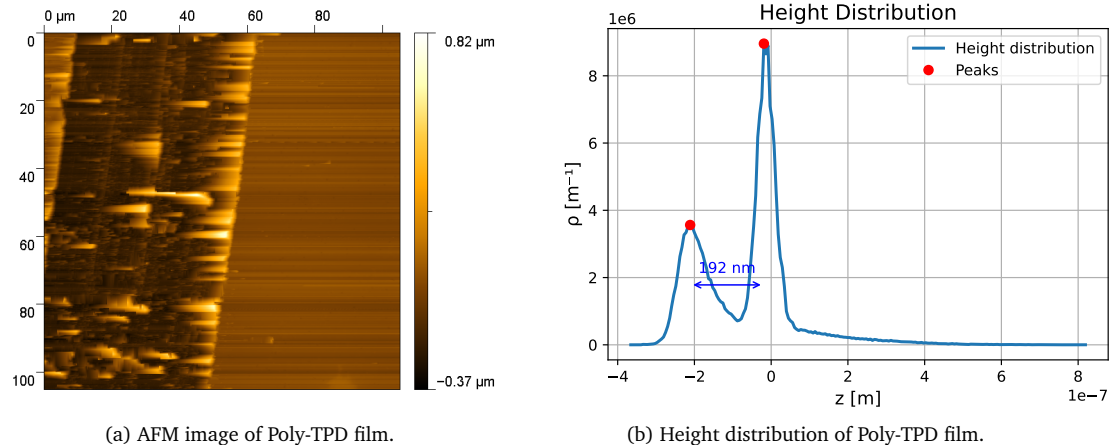
I hereby declare that I have completed the present work independently and without any unauthorized assistance or use of sources other than those specified. I affirm that no third party has received any monetary compensation from me, either directly or indirectly, for work related to the content of this bachelor thesis, and that the submitted work has not been presented in the same or a similar form to any other examination authority, either domestically or abroad, for the purpose of obtaining a degree or other certification. All material taken from other sources or from other individuals that has been used in this work or directly referenced has been clearly marked as such. In particular, all individuals who directly contributed to the creation of this work have been acknowledged.

Leipzig, September 17, 2024

Federico Porcelli

Appendix A

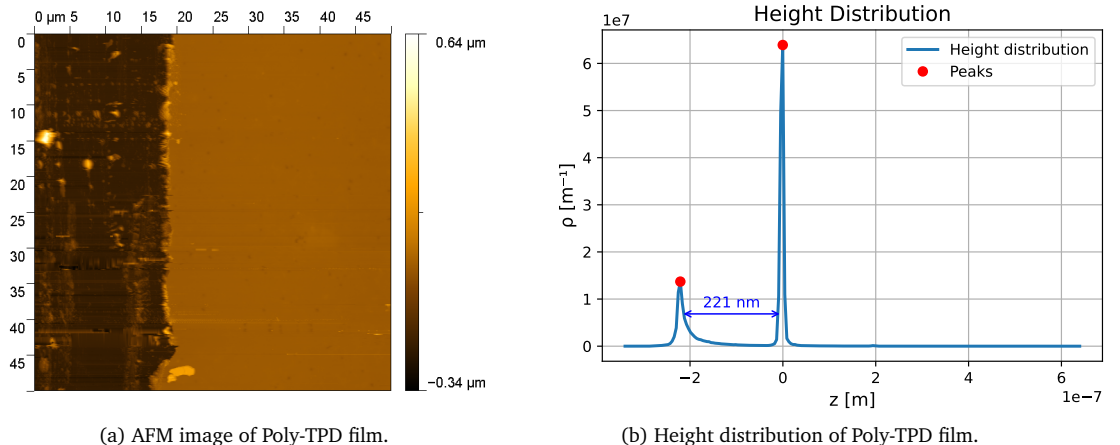
AFM Data



(a) AFM image of Poly-TPD film.

(b) Height distribution of Poly-TPD film.

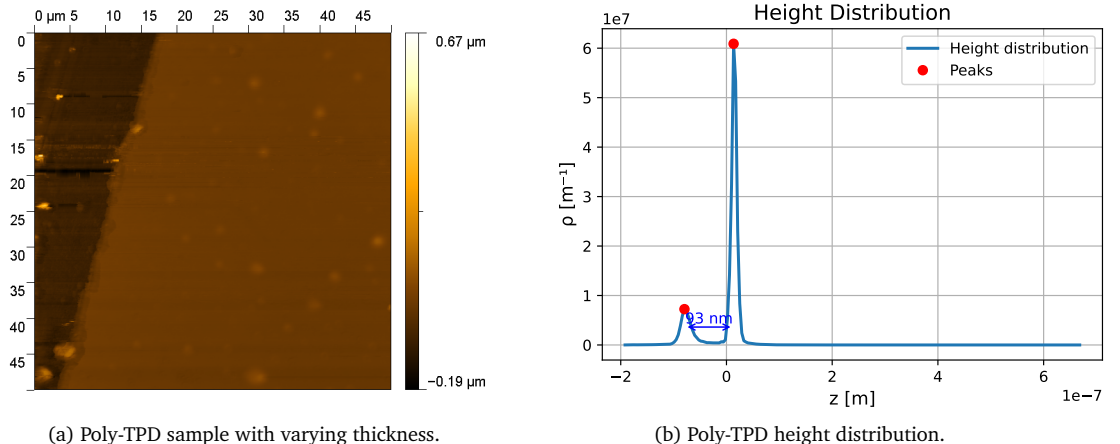
Figure A.1: Poly-TPD thin film: AFM image and height distribution (c.a. 200nm).



(a) AFM image of Poly-TPD film.

(b) Height distribution of Poly-TPD film.

Figure A.2: Poly-TPD thin film: AFM image and height distribution (c.a. 200nm).



(a) Poly-TPD sample with varying thickness.

(b) Poly-TPD height distribution.

Figure A.3: Poly-TPD thin film with varying thickness: AFM image and height distribution (c.a. 110nm).

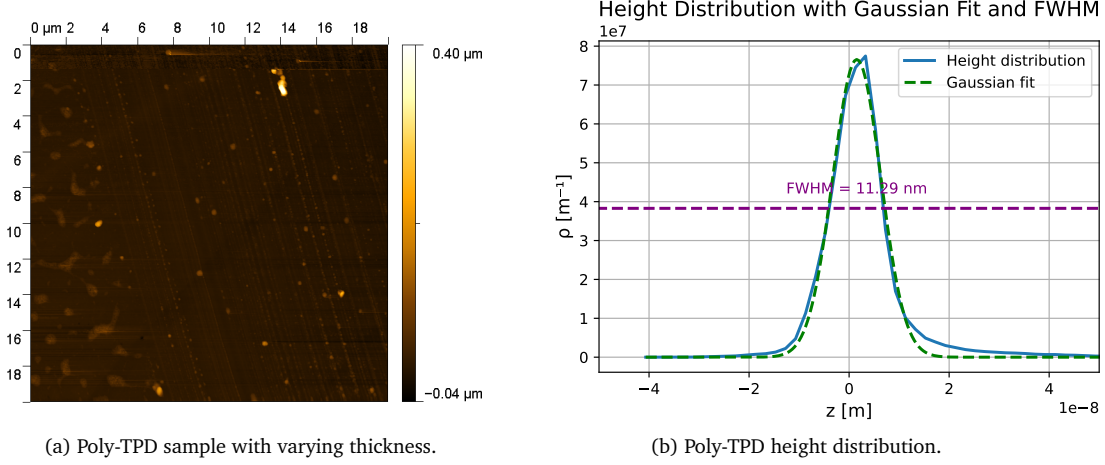


Figure A.4: Poly-TPD thin film with varying thickness: AFM image and height distribution (c.a. 24nm).

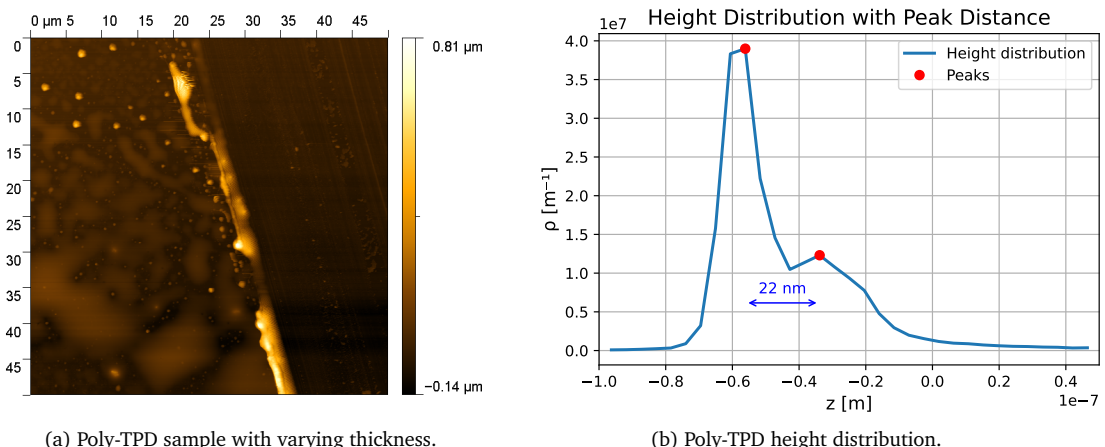


Figure A.5: Poly-TPD thin film with varying thickness: AFM image and height distribution (c.a. 8nm).

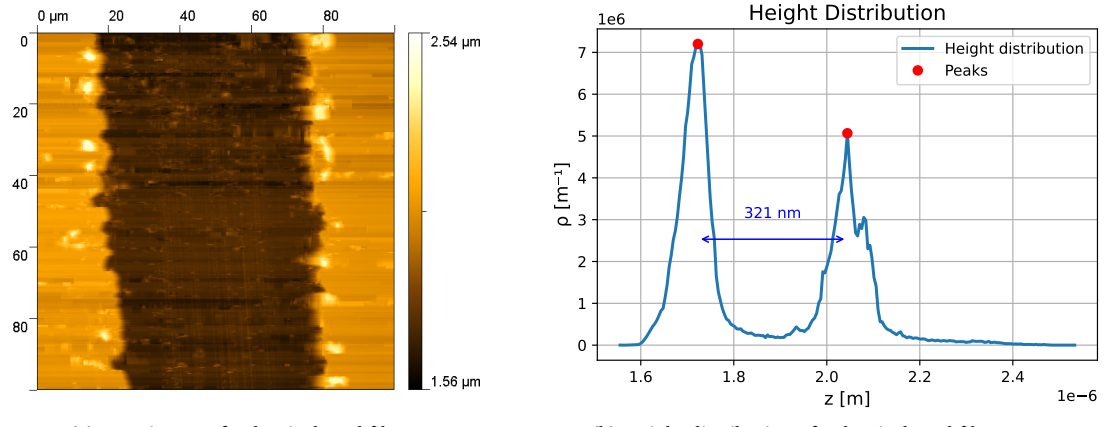


Figure A.6: Poly-Bisphenol thin film: AFM image and height distribution (c.a. 320nm).

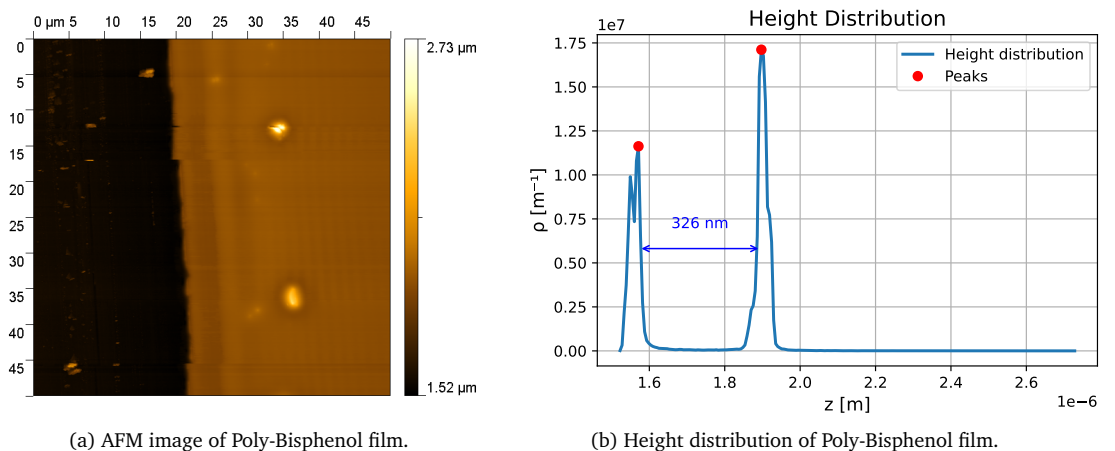


Figure A.7: Poly-Bisphenol thin film: AFM image and height distribution (c.a. 320nm).

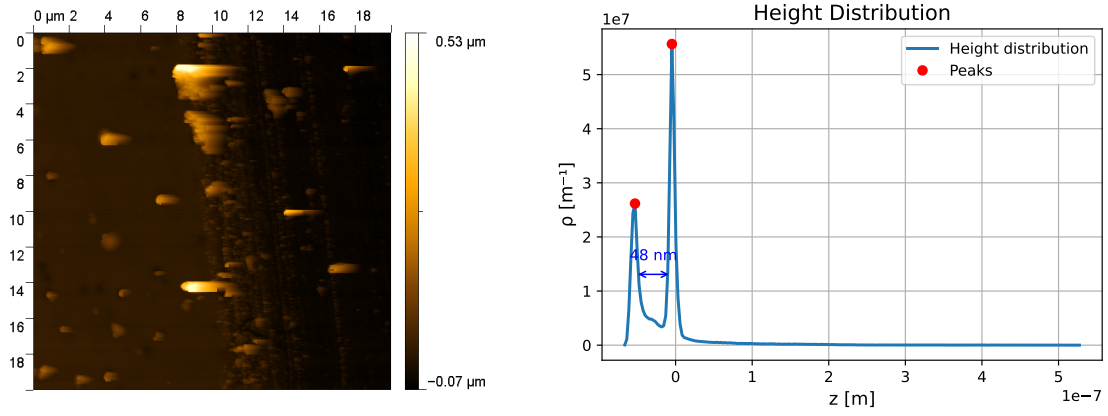


Figure A.8: Poly-Bisphenol thin film: AFM image and height distribution (c.a. 43nm).

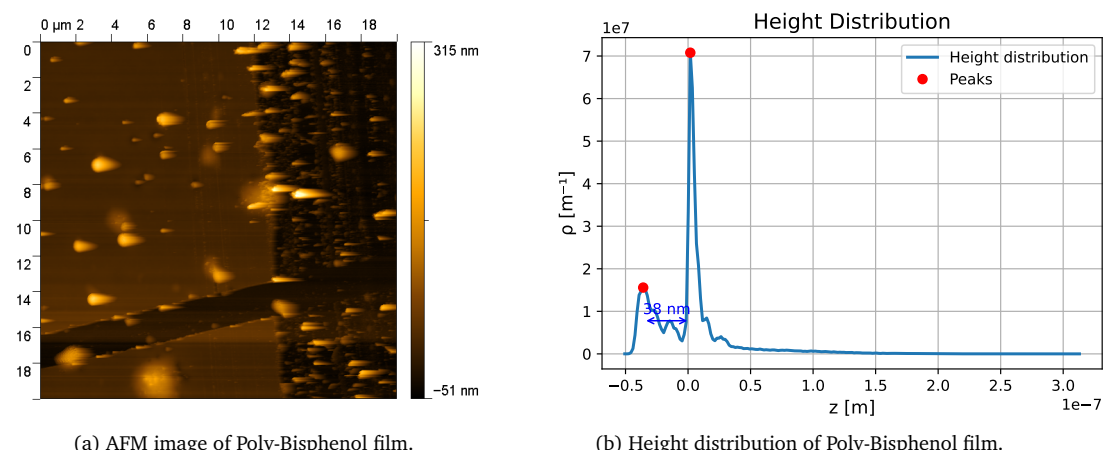
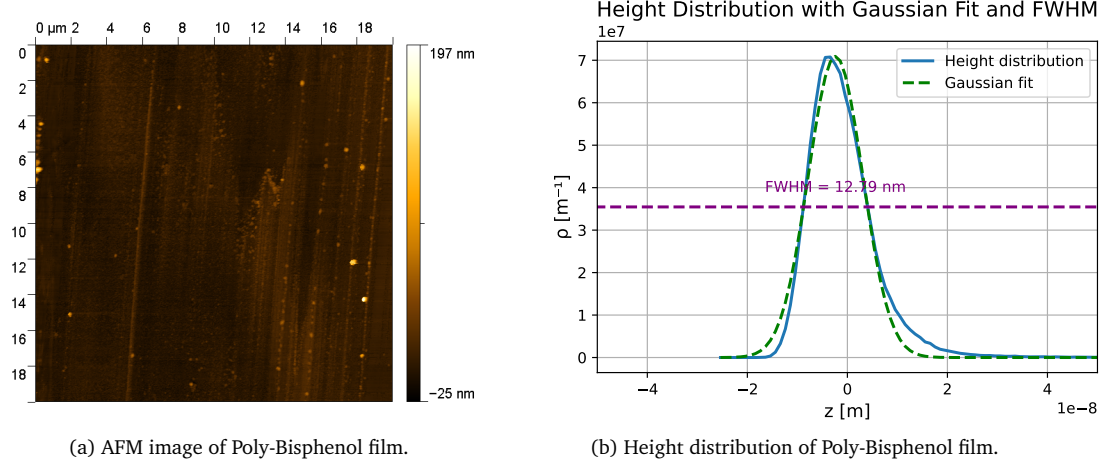


Figure A.9: Poly-Bisphenol thin film: AFM image and height distribution (c.a. 43nm).



(a) AFM image of Poly-Bisphenol film.

(b) Height distribution of Poly-Bisphenol film.

Figure A.10: Poly-Bisphenol thin film: AFM image and height distribution (c.a. 14nm).

Appendix B

BDS Data

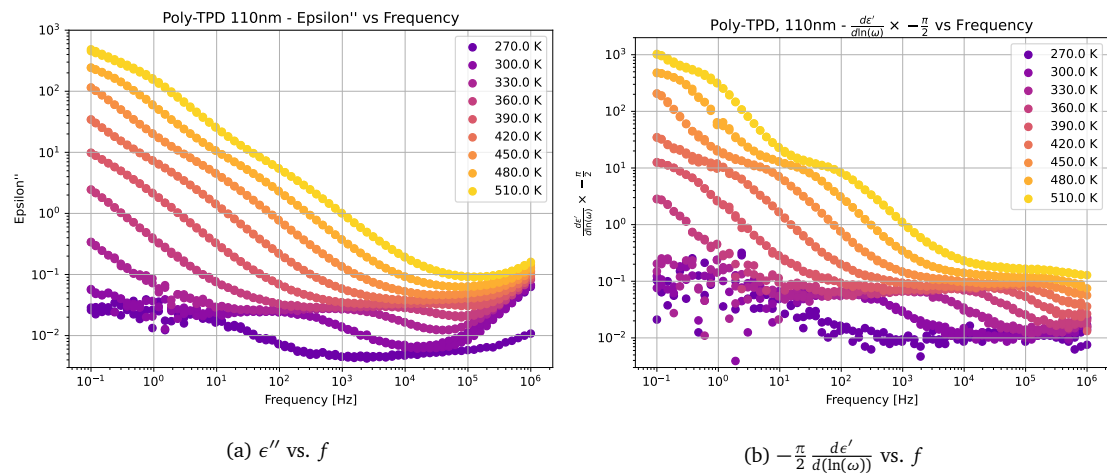


Figure B.1: 110nm Poly-TPD thin film

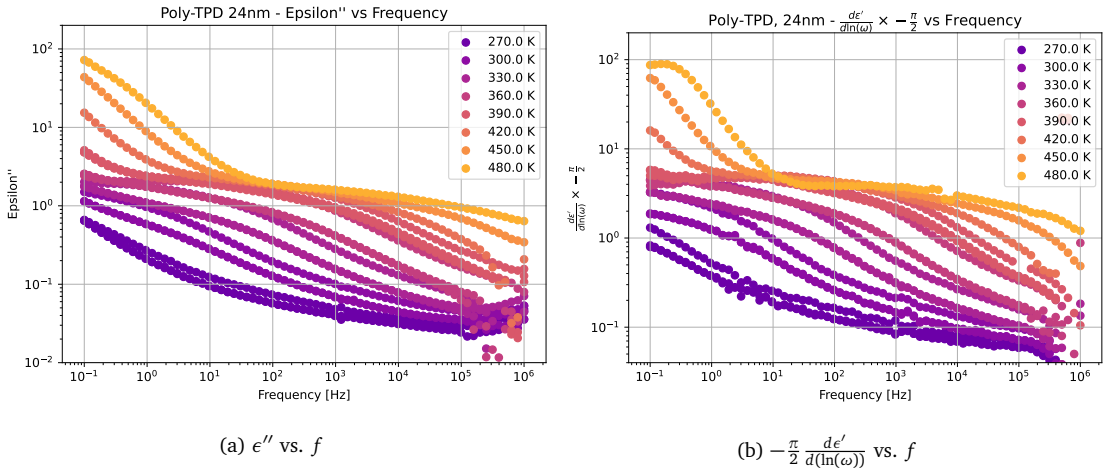


Figure B.2: 24nm Poly-TPD thin film

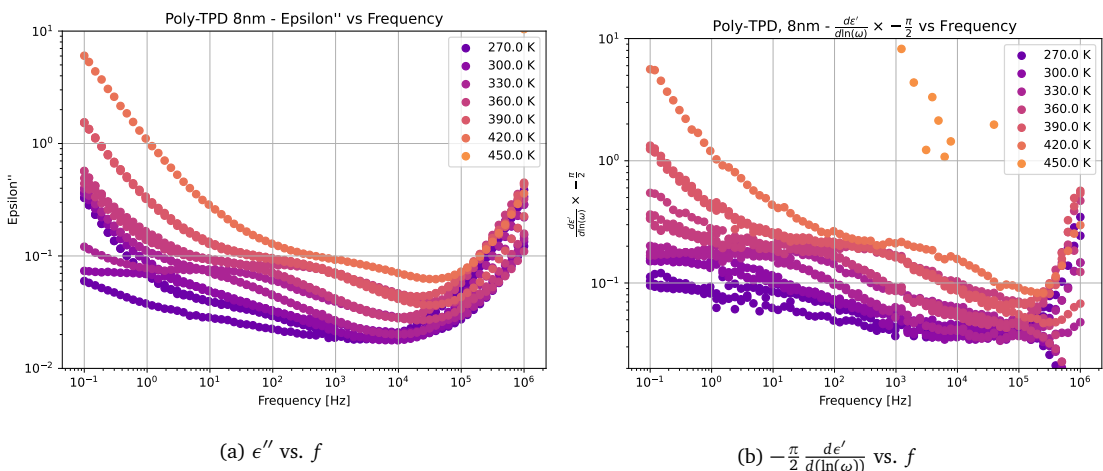


Figure B.3: 8nm Poly-TPD thin film

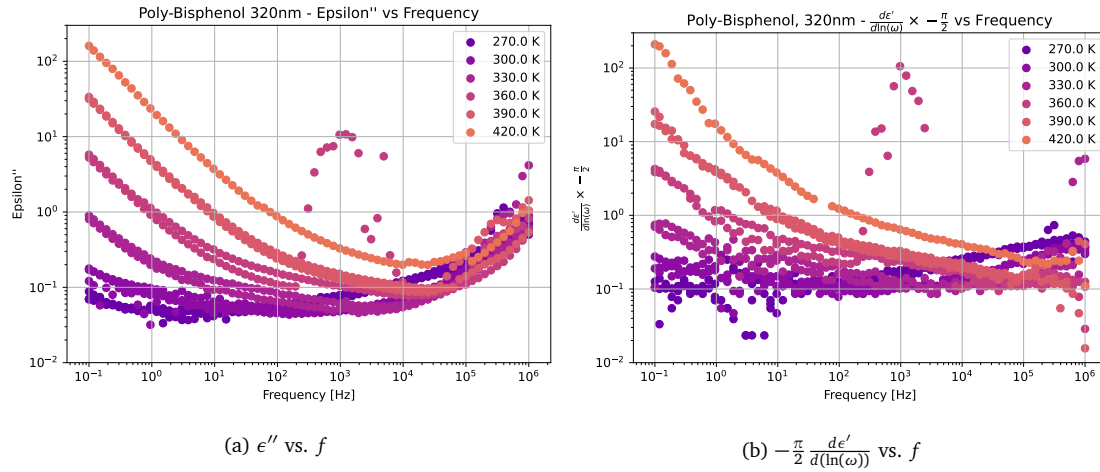


Figure B.4: 320nm Poly-Bisphenol thin film

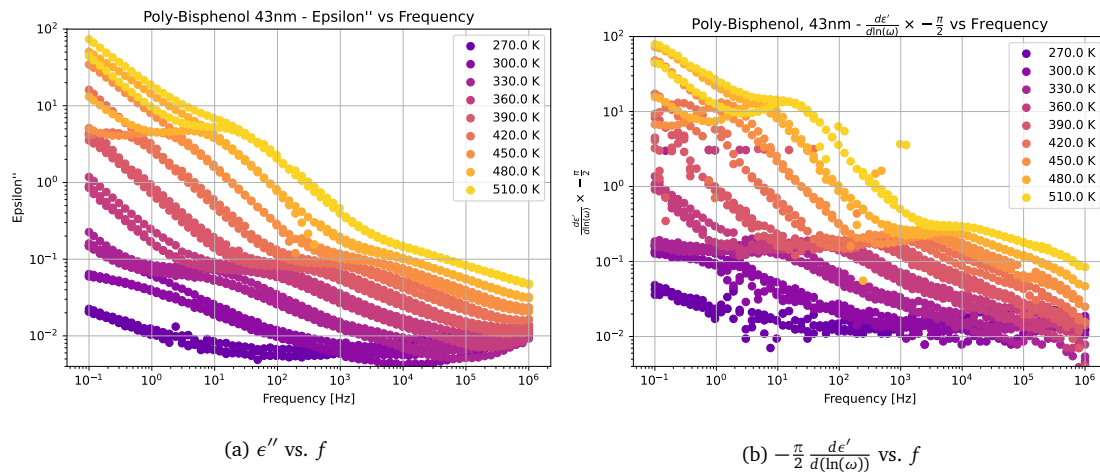


Figure B.5: 43nm Poly-Bisphenol thin film

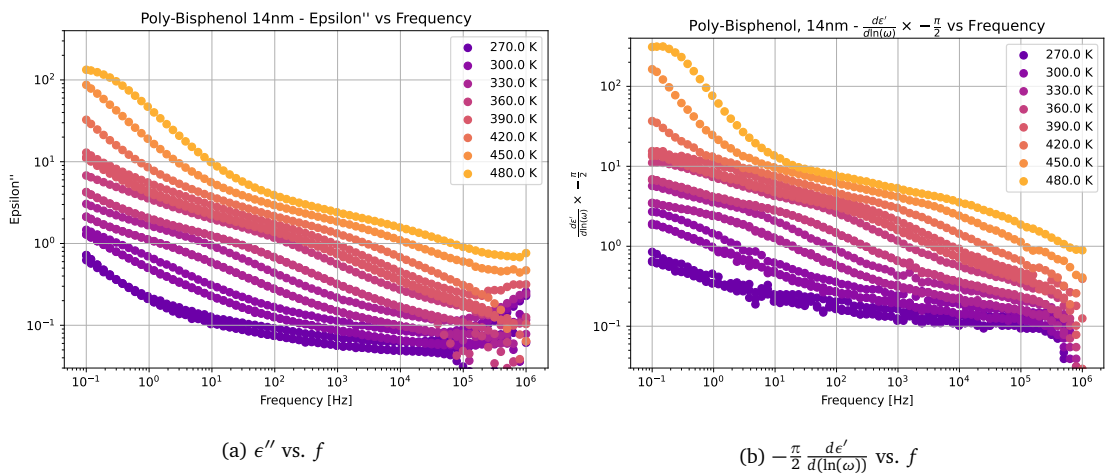
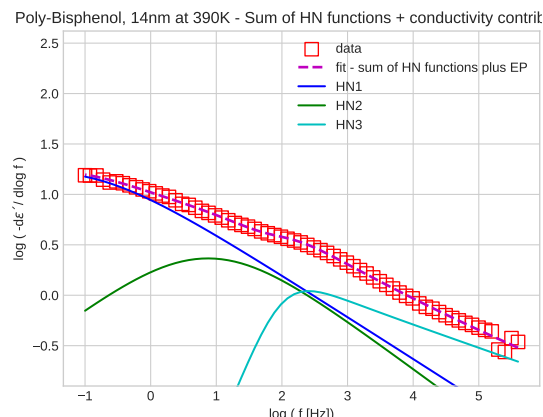


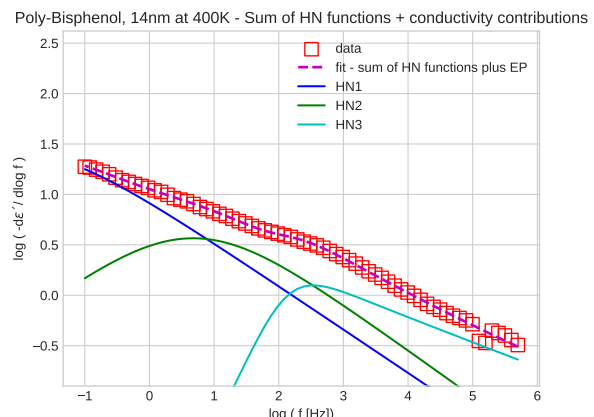
Figure B.6: 14nm Poly-Bisphenol thin film

Appendix C

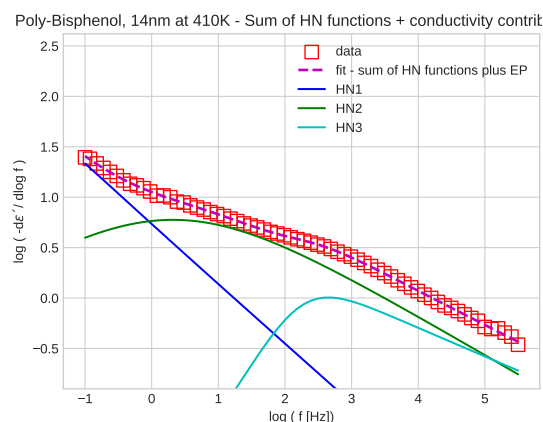
Fits of BDS Data



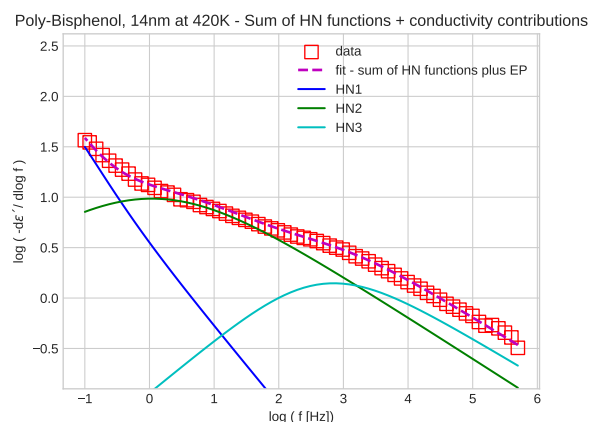
(a) Poly-Bisphenol, 14nm, 390K



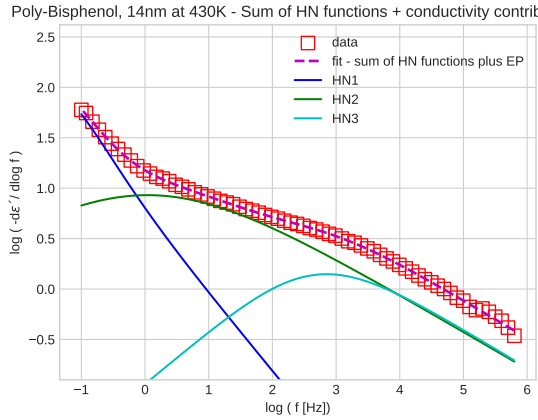
(b) Poly-Bisphenol, 14nm, 400K



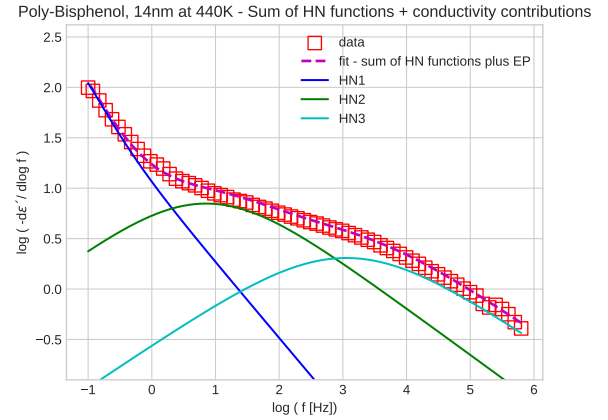
(a) Poly-Bisphenol, 14nm, 410K



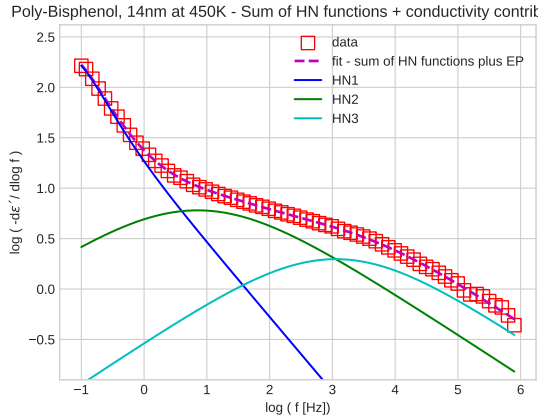
(b) Poly-Bisphenol, 14nm, 420K



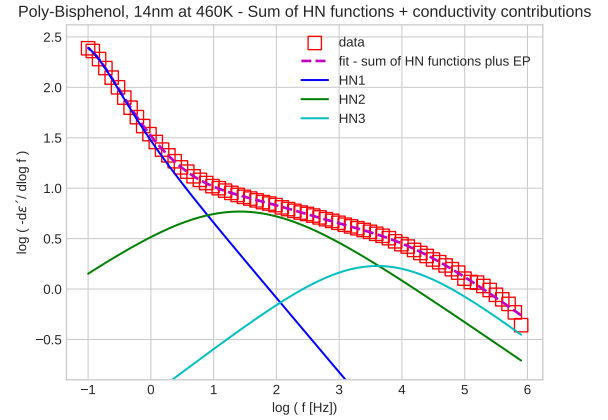
(a) Poly-Bisphenol, 14nm, 430K



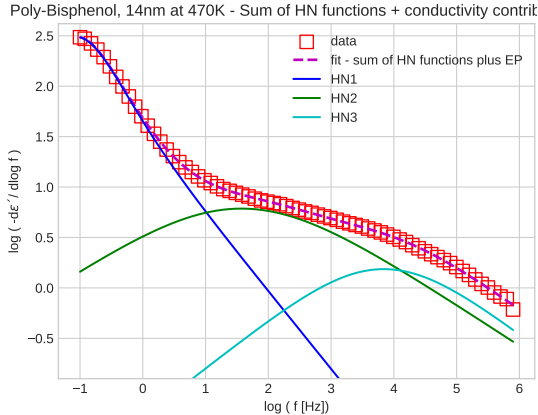
(b) Poly-Bisphenol, 14nm, 440K



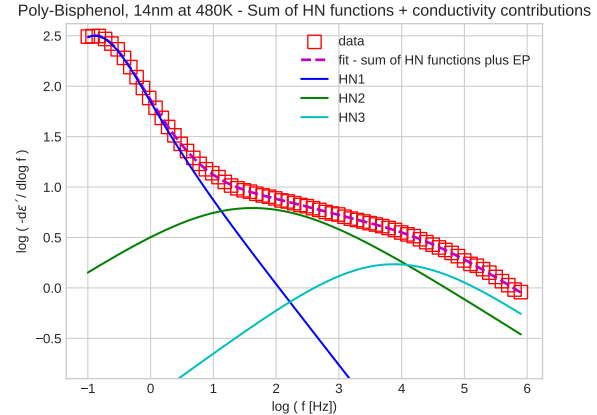
(a) Poly-Bisphenol, 14nm, 450K



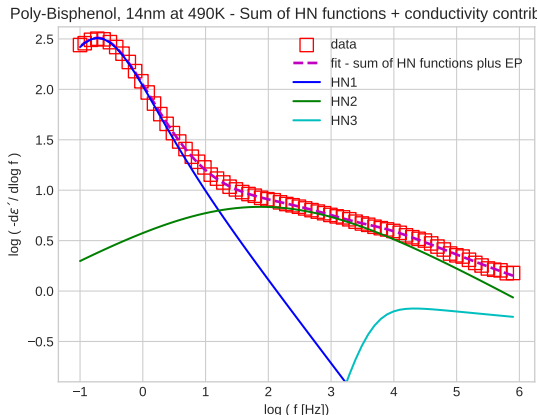
(b) Poly-Bisphenol, 14nm, 460K



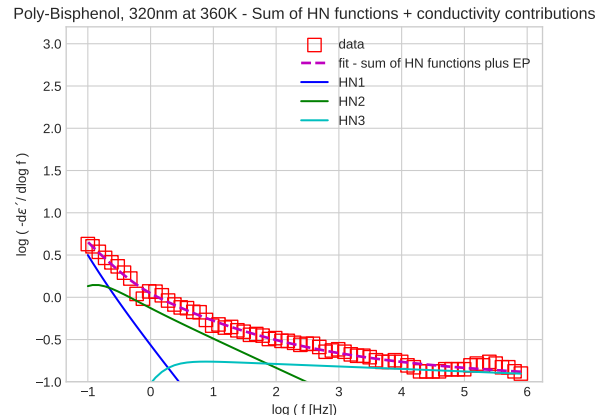
(a) Poly-Bisphenol, 14nm, 470K



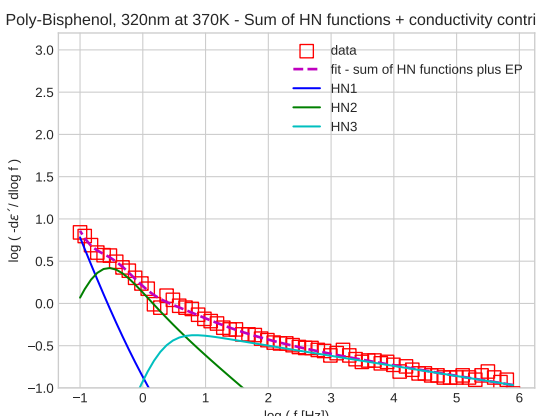
(b) Poly-Bisphenol, 14nm, 480K



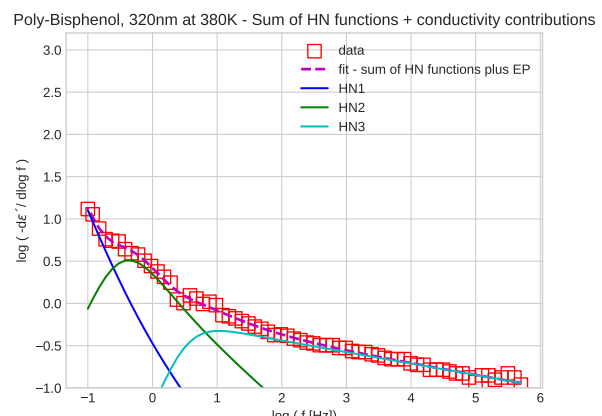
(a) Poly-Bisphenol, 14nm, 490K



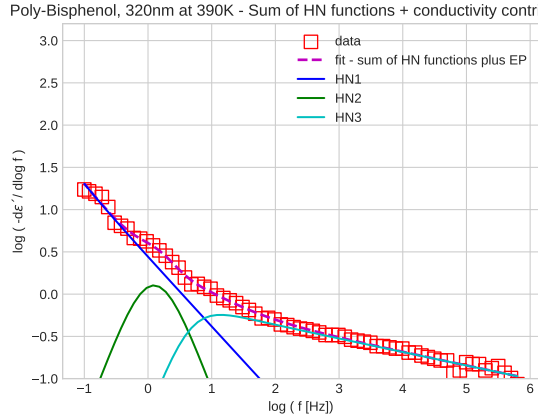
(b) Poly-Bisphenol, 14nm, 360K



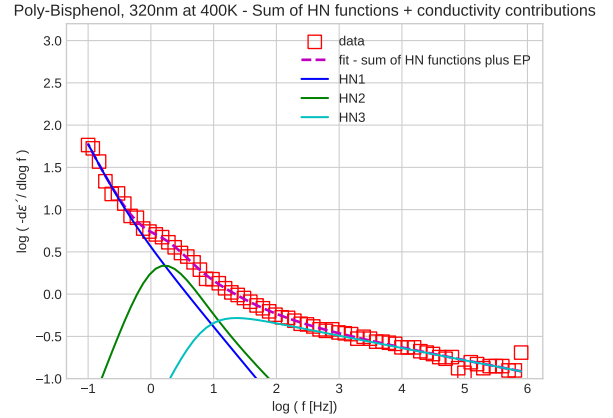
(a) Poly-Bisphenol, 320nm, 370K



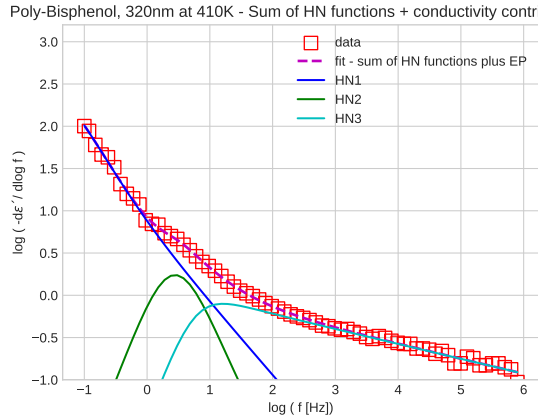
(b) Poly-Bisphenol, 320nm, 380K



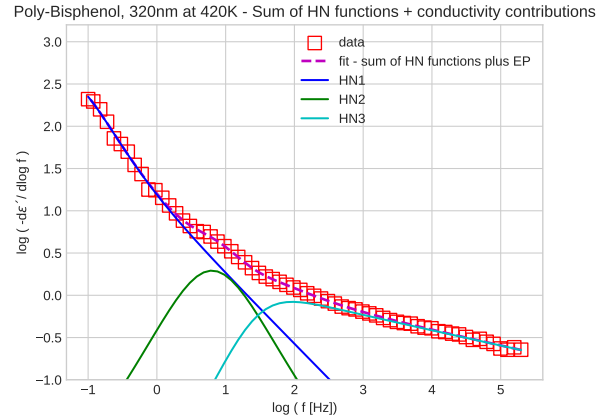
(a) Poly-Bisphenol, 320nm, 390K



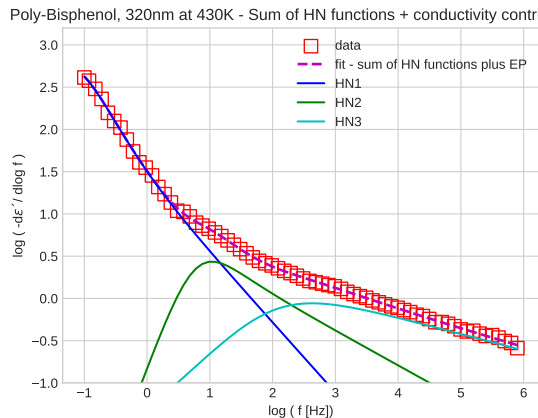
(b) Poly-Bisphenol, 320nm, 400K



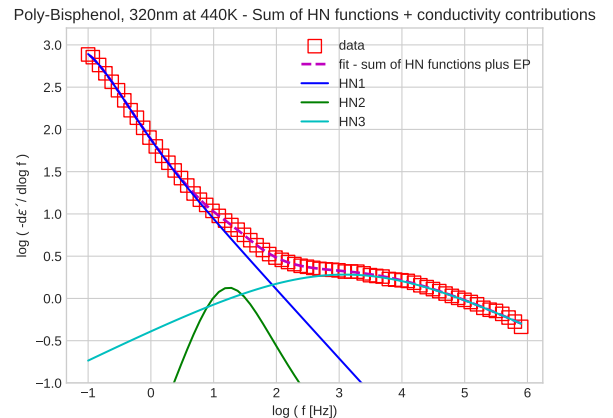
(a) Poly-Bisphenol, 320nm, 410K



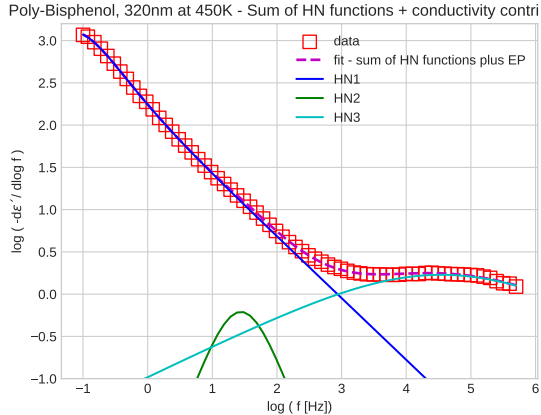
(b) Poly-Bisphenol, 320nm, 420K



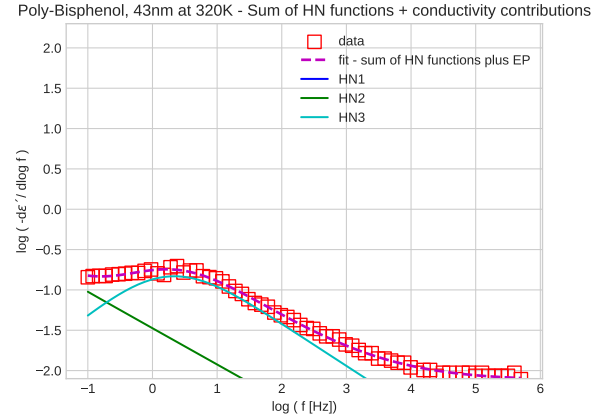
(a) Poly-Bisphenol, 320nm, 430K



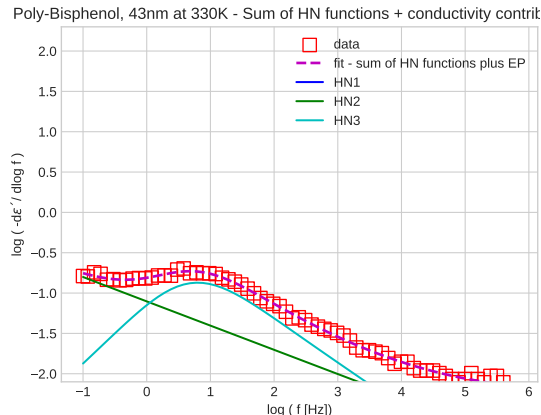
(b) Poly-Bisphenol, 320nm, 440K



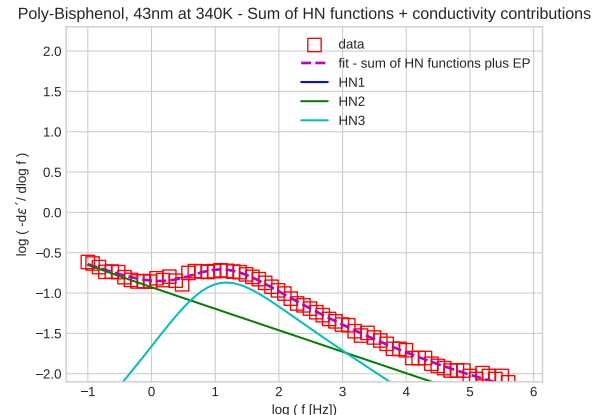
(a) Poly-Bisphenol, 320nm, 450K



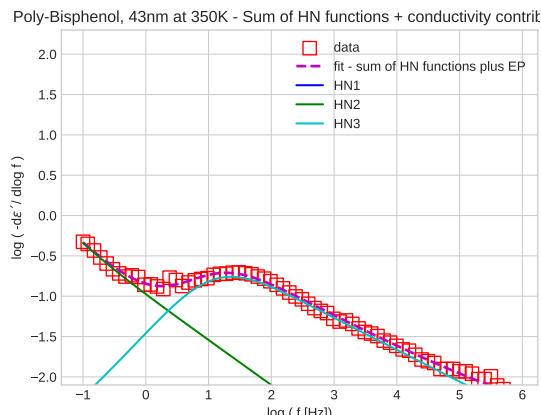
(b) Poly-Bisphenol, 320nm, 320K



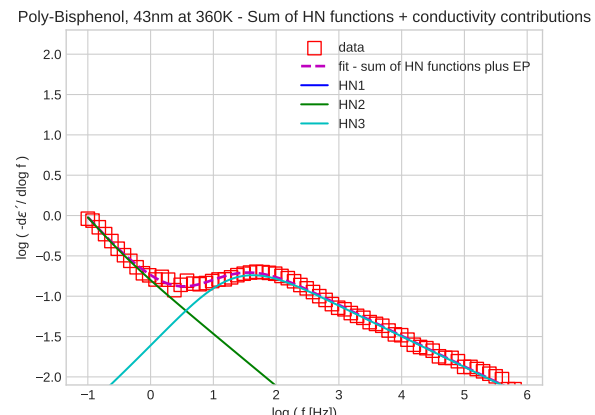
(a) Poly-Bisphenol, 43nm, 330K



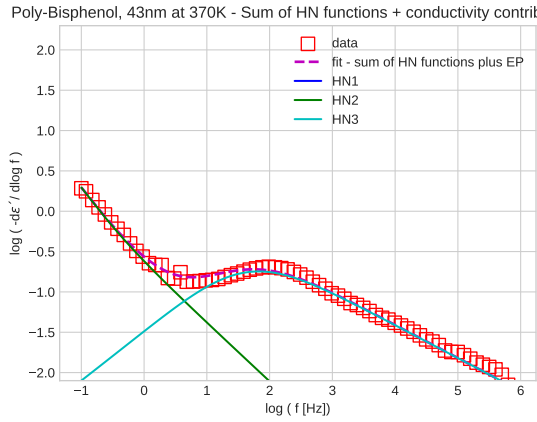
(b) Poly-Bisphenol, 43nm, 340K



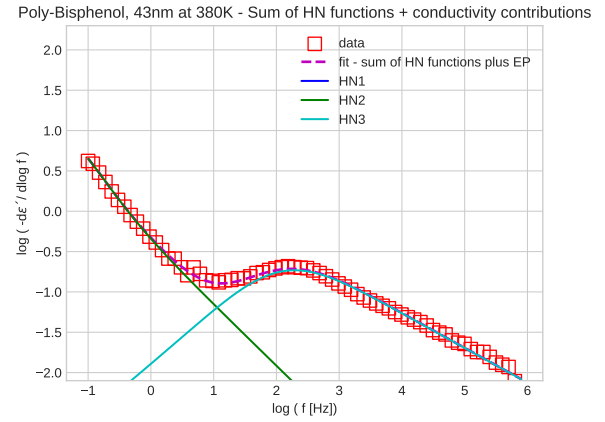
(a) Poly-Bisphenol, 43nm, 350K



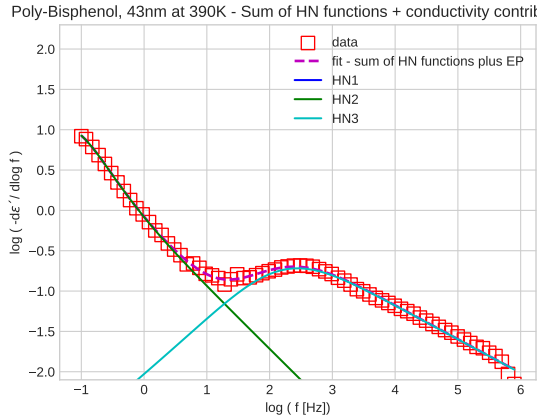
(b) Poly-Bisphenol, 43nm, 360K



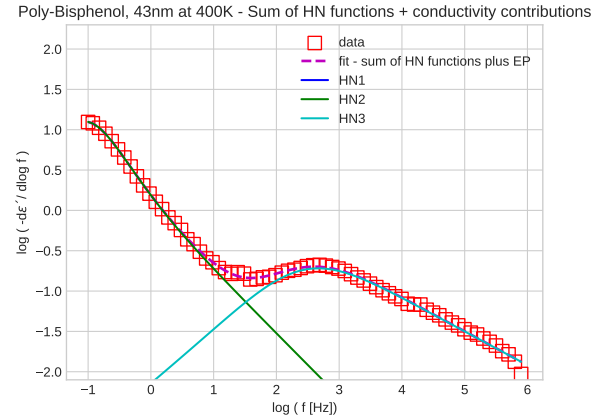
(a) Poly-Bisphenol, 43nm, 370K



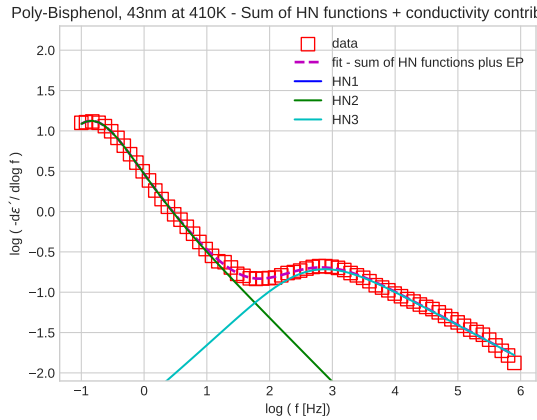
(b) Poly-Bisphenol, 43nm, 380K



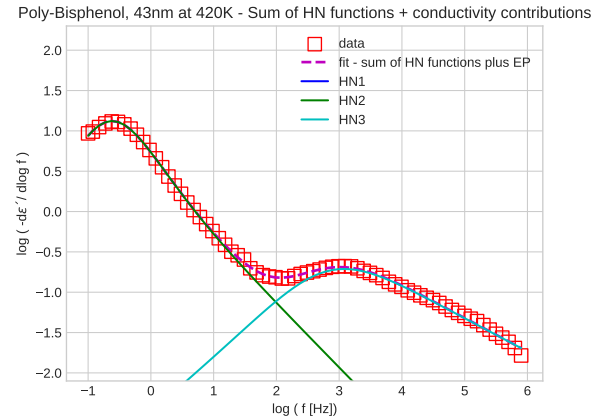
(a) Poly-Bisphenol, 43nm, 390K



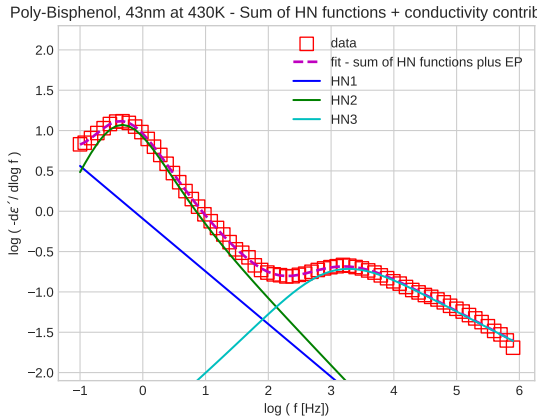
(b) Poly-Bisphenol, 43nm, 400K



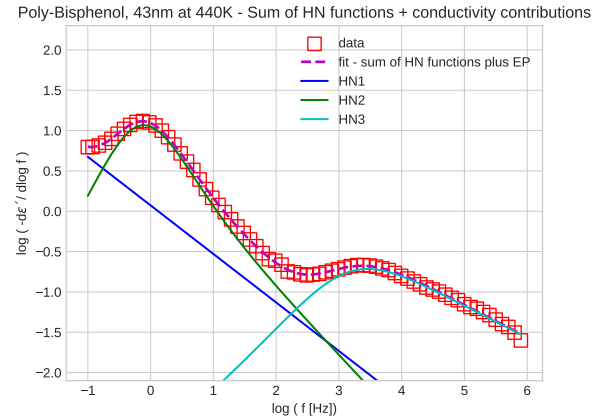
(a) Poly-Bisphenol, 43nm, 410K



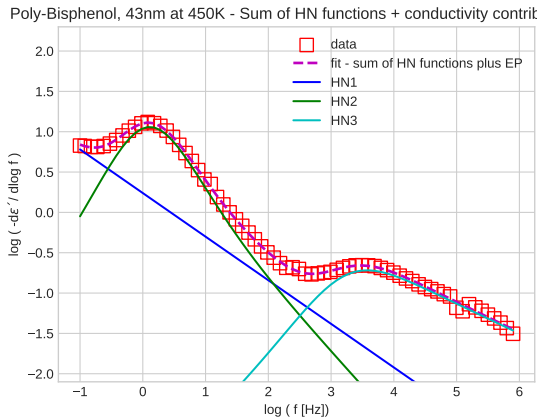
(b) Poly-Bisphenol, 43nm, 420K



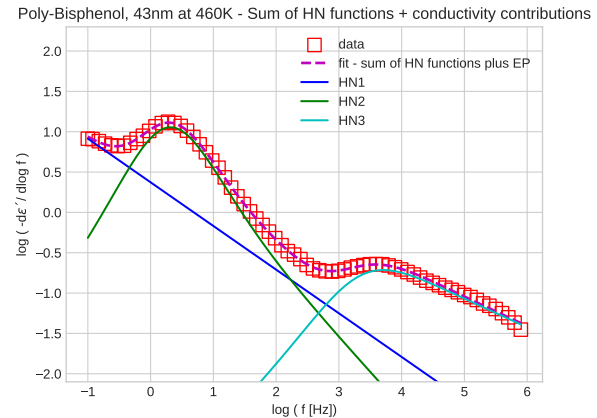
(a) Poly-Bisphenol, 43nm, 430K



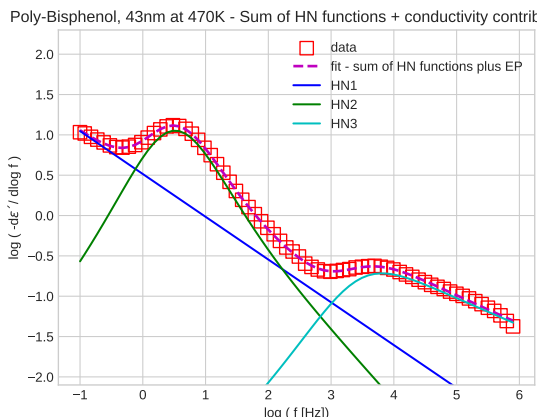
(b) Poly-Bisphenol, 43nm, 440K



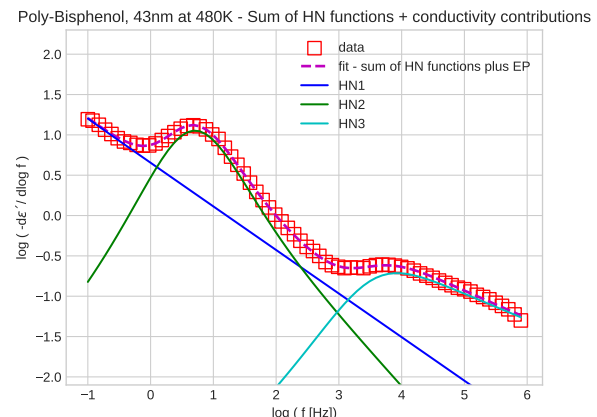
(a) Poly-Bisphenol, 43nm, 450K



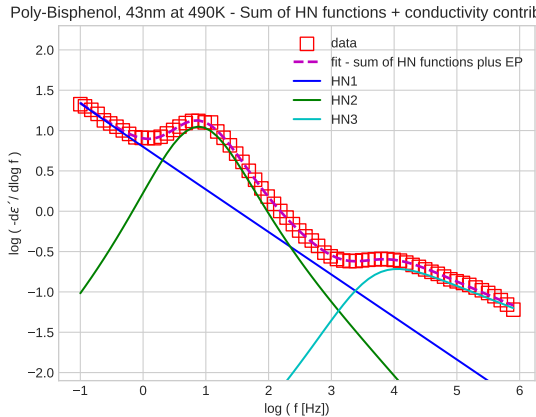
(b) Poly-Bisphenol, 43nm, 460K



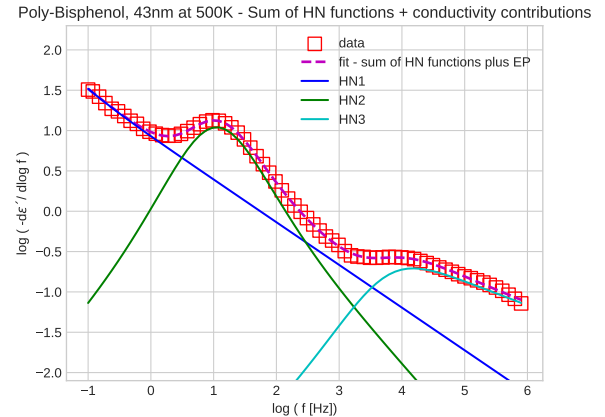
(a) Poly-Bisphenol, 43nm, 470K



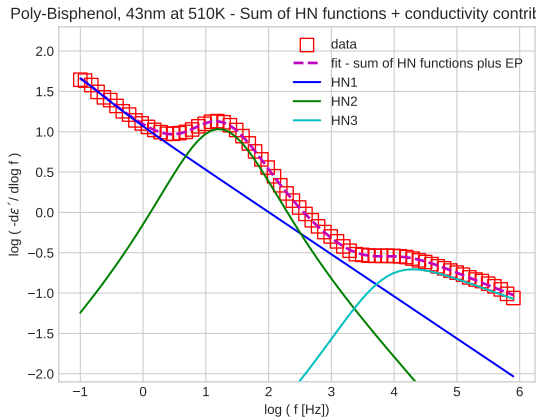
(b) Poly-Bisphenol, 43nm, 480K



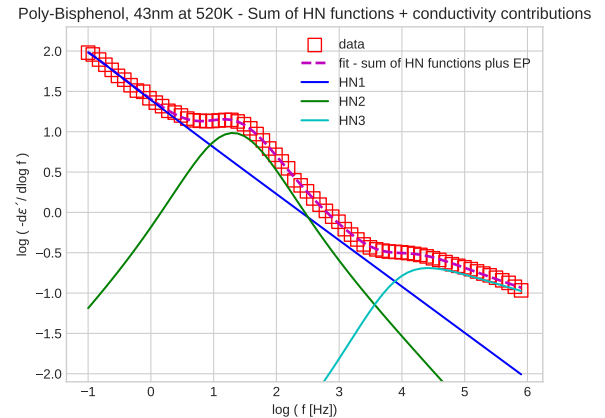
(a) Poly-Bisphenol, 43nm, 490K



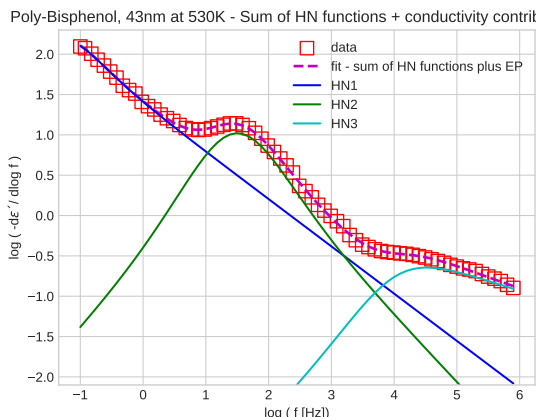
(b) Poly-Bisphenol, 43nm, 500K



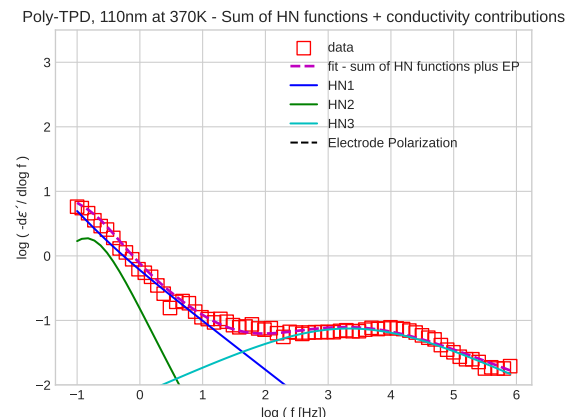
(a) Poly-Bisphenol, 43nm, 510K



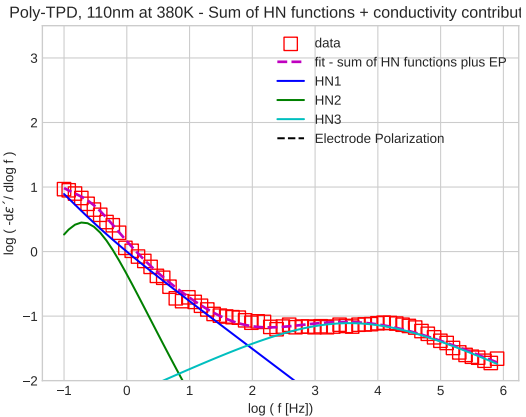
(b) Poly-Bisphenol, 43nm, 520K



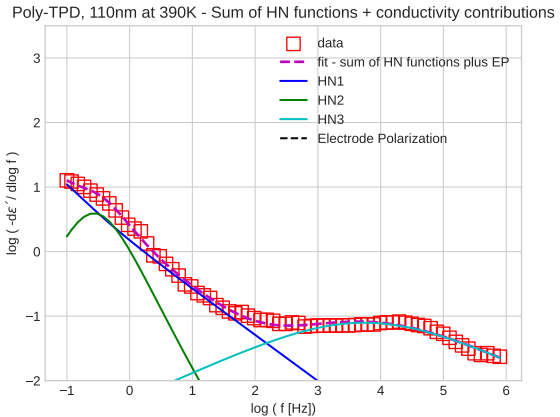
(a) Poly-Bisphenol, 43nm, 530K



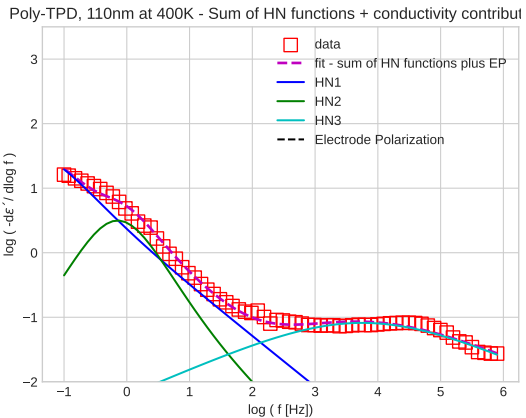
(b) Poly-Bisphenol, 43nm, 370K



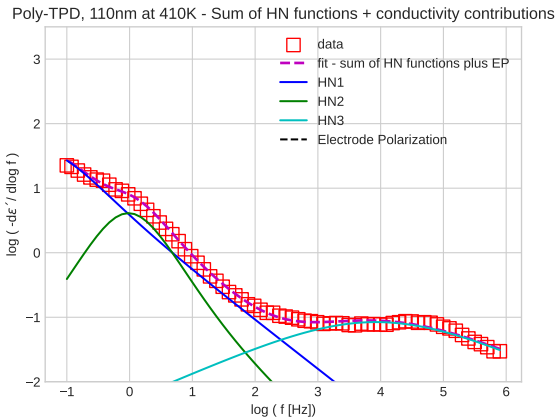
(a) Poly-TPD, 110nm, 380K



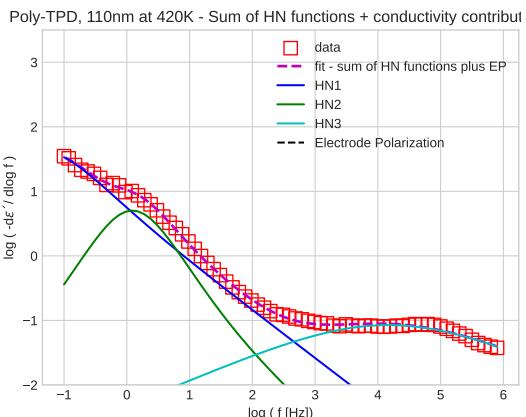
(b) Poly-TPD, 110nm, 390K



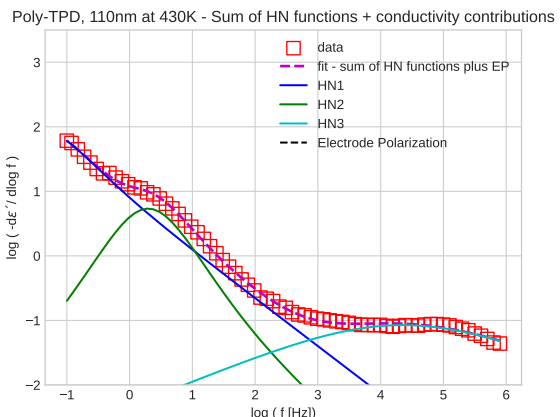
(a) Poly-TPD, 110nm, 400K



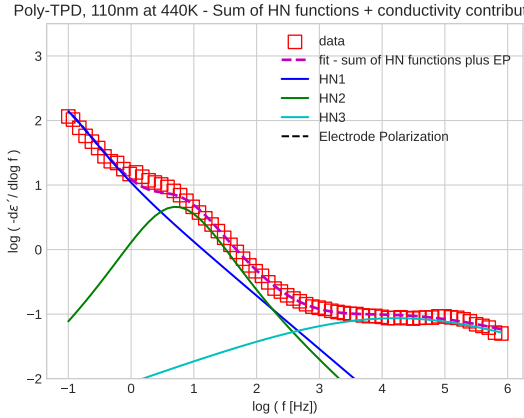
(b) Poly-TPD, 110nm, 410K



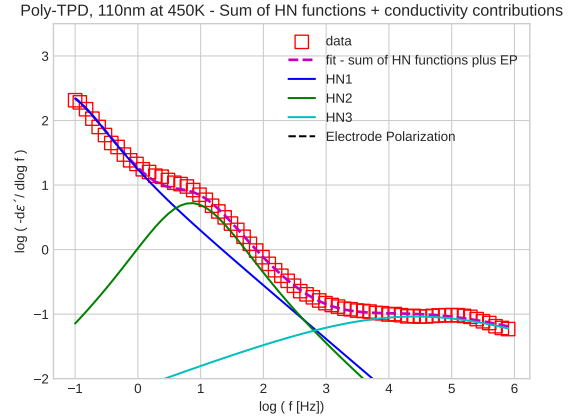
(a) Poly-TPD, 110nm, 420K



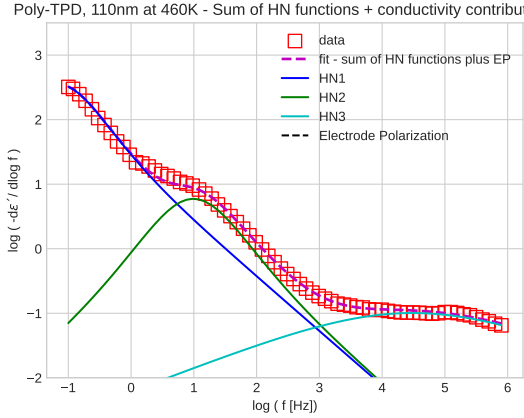
(b) Poly-TPD, 110nm, 430K



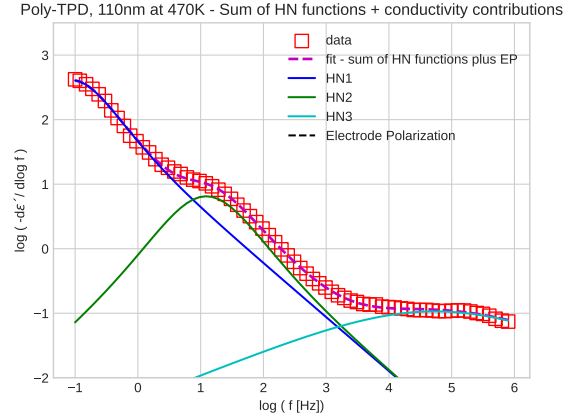
(a) Poly-TPD, 110nm, 440K



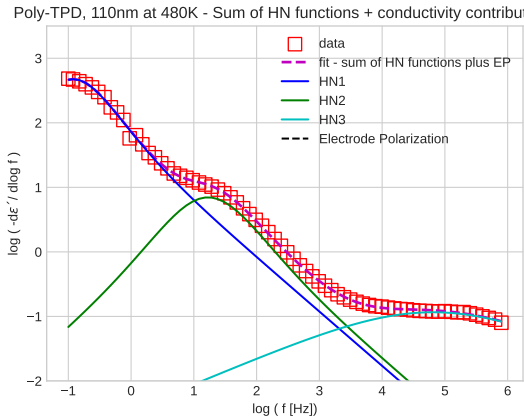
(b) Poly-TPD, 110nm, 450K



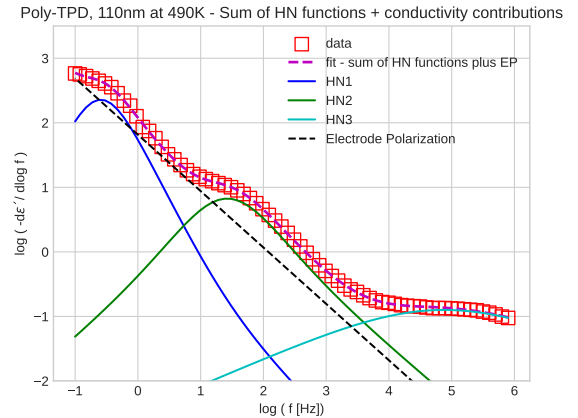
(a) Poly-TPD, 110nm, 460K



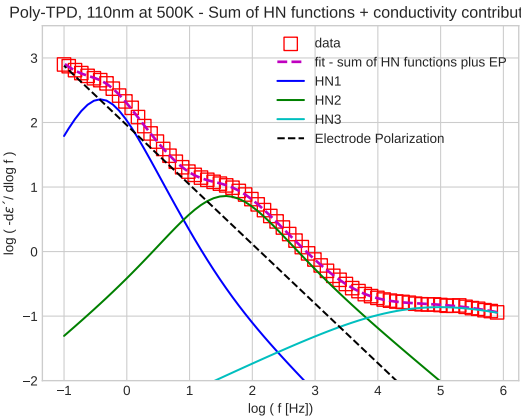
(b) Poly-TPD, 110nm, 470K



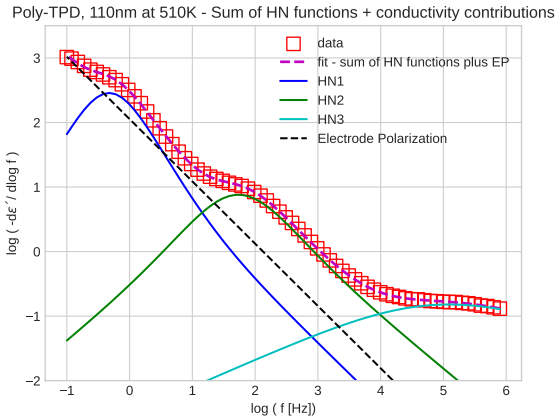
(a) Poly-TPD, 110nm, 480K



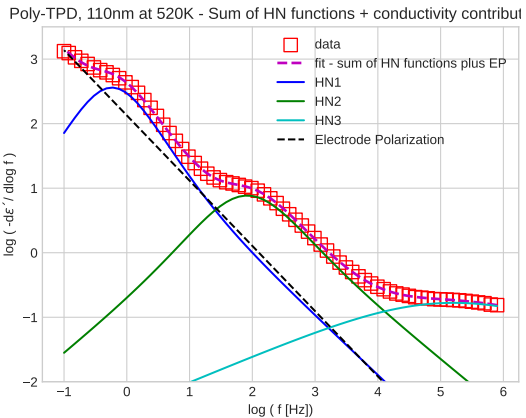
(b) Poly-TPD, 110nm, 490K



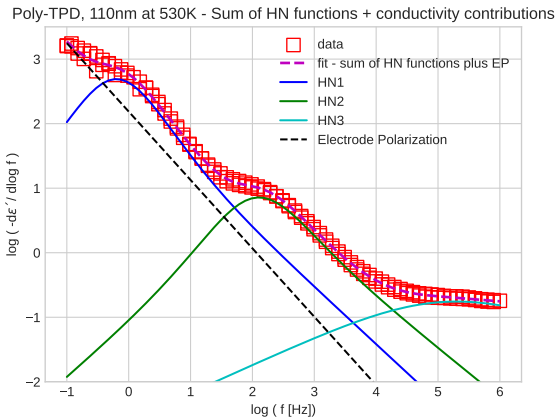
(a) Poly-TPD, 110nm, 500K



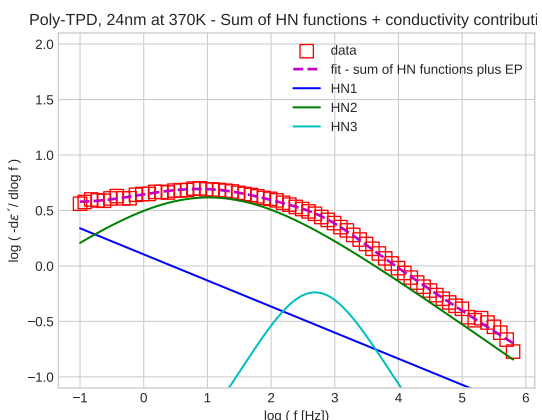
(b) Poly-TPD, 110nm, 510K



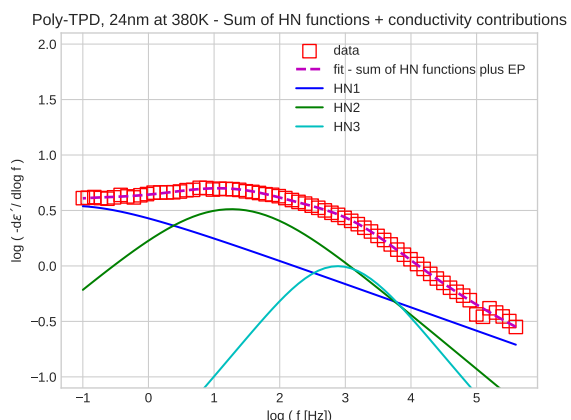
(a) Poly-TPD, 110nm, 520K



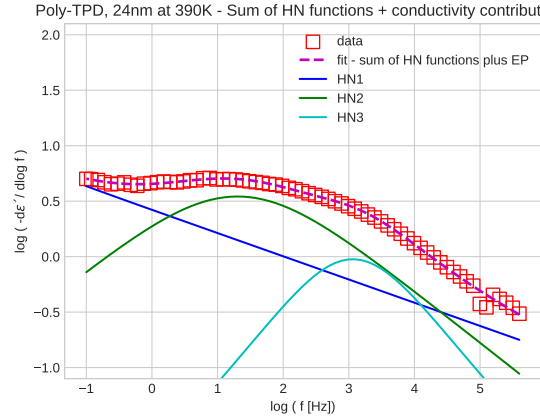
(b) Poly-TPD, 110nm, 530K



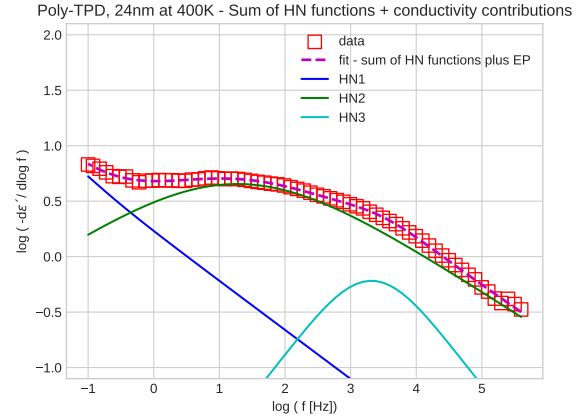
(a) Poly-TPD, 24nm, 370K



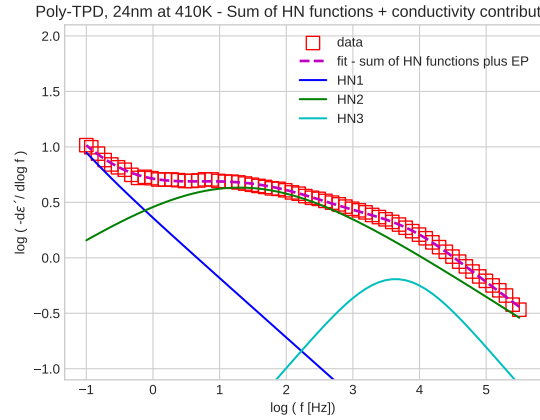
(b) Poly-TPD, 24nm, 380K



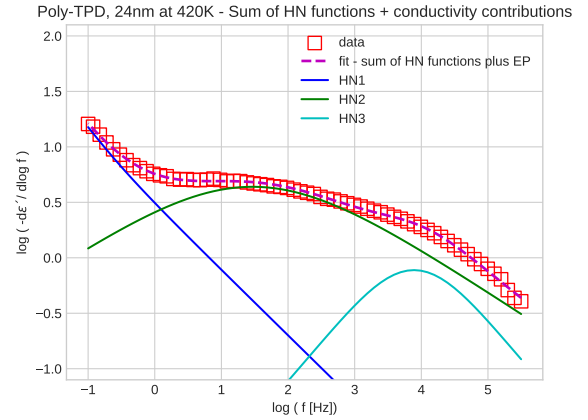
(a) Poly-TPD, 24nm, 390K



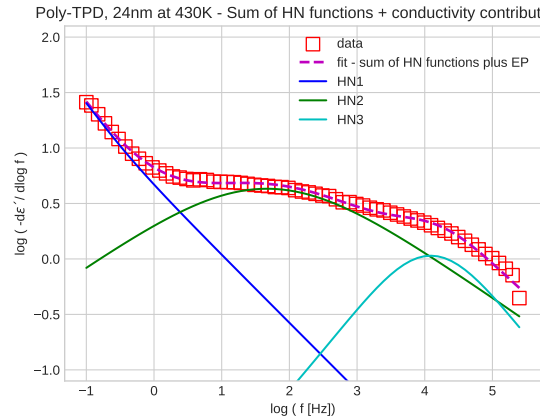
(b) Poly-TPD, 24nm, 400K



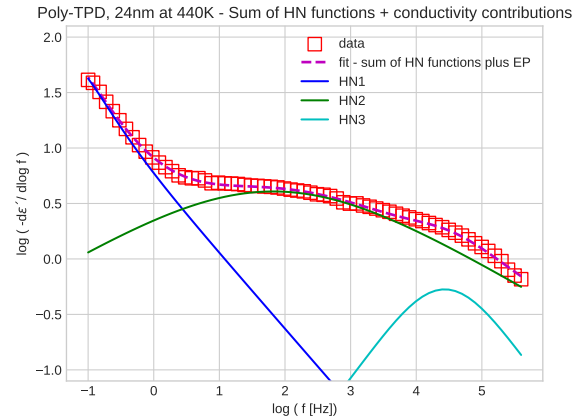
(a) Poly-TPD, 24nm, 410K



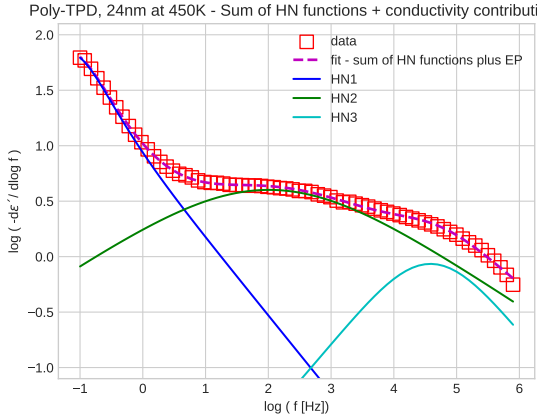
(b) Poly-TPD, 24nm, 420K



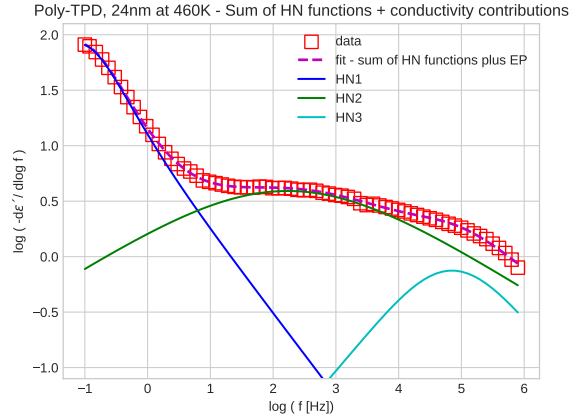
(a) Poly-TPD, 24nm, 430K



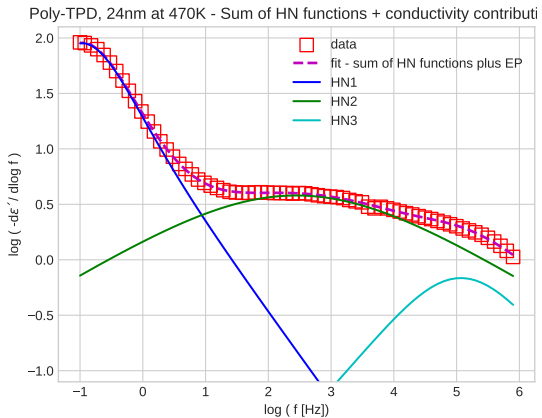
(b) Poly-TPD, 24nm, 440K



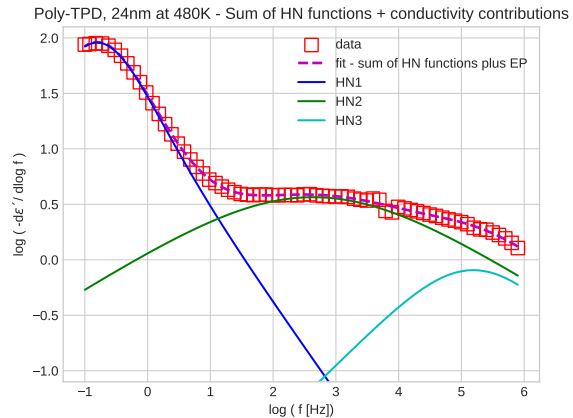
(a) Poly-TPD, 24nm, 450K



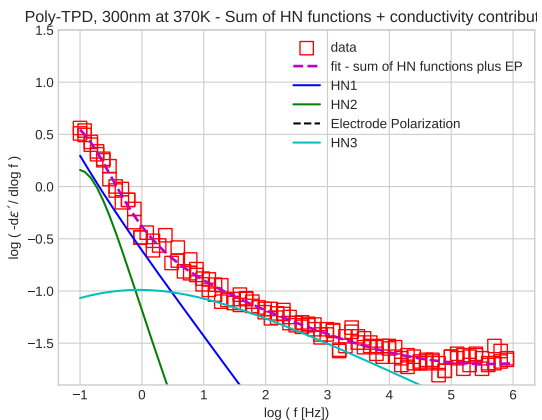
(b) Poly-TPD, 24nm, 460K



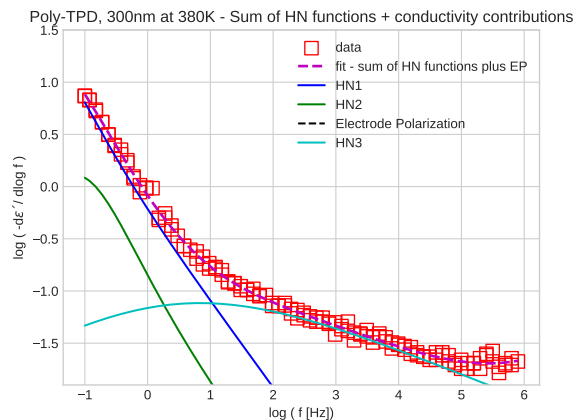
(a) Poly-TPD, 24nm, 470K



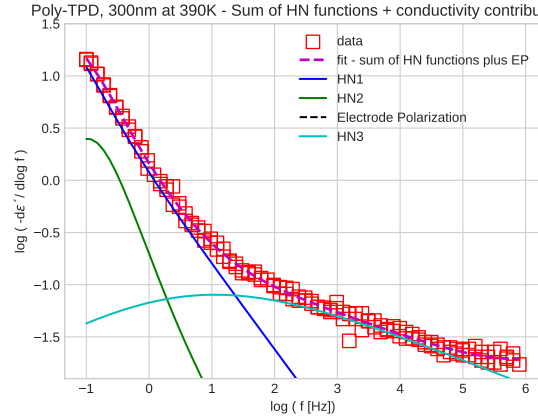
(b) Poly-TPD, 24nm, 480K



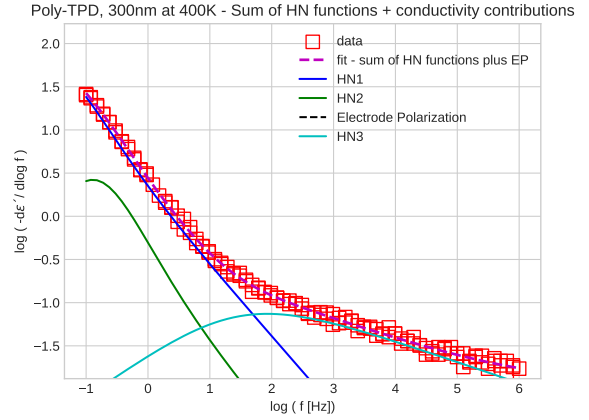
(a) Poly-TPD, 300nm, 370K



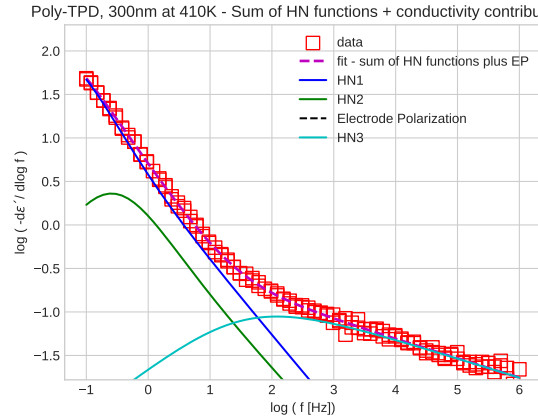
(b) Poly-TPD, 300nm, 380K



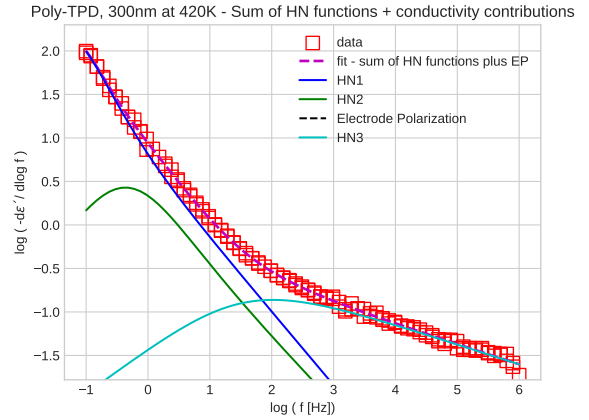
(a) Poly-TPD, 300nm, 390K



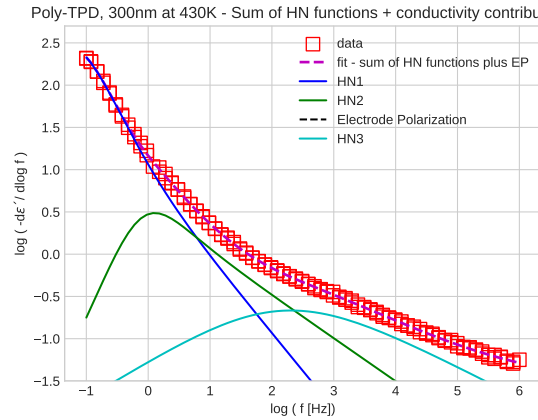
(b) Poly-TPD, 300nm, 400K



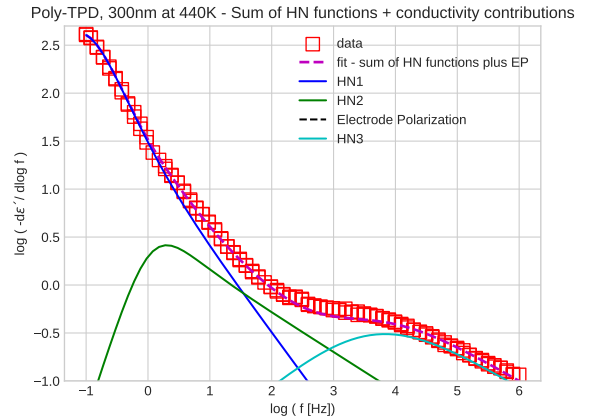
(a) Poly-TPD, 300nm, 410K



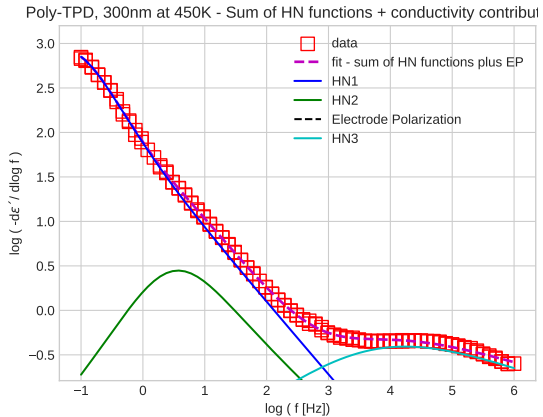
(b) Poly-TPD, 300nm, 420K



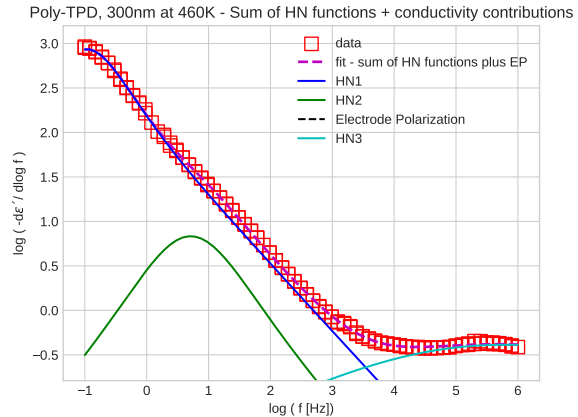
(a) Poly-TPD, 300nm, 430K



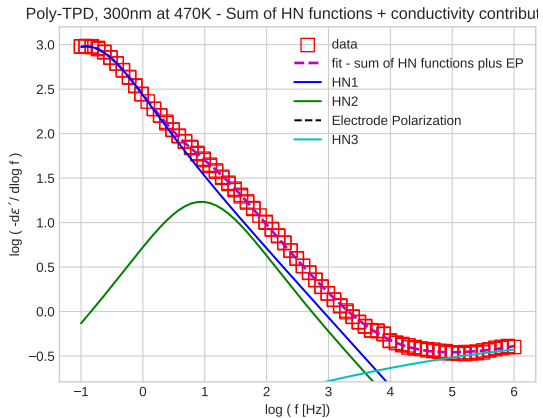
(b) Poly-TPD, 300nm, 440K



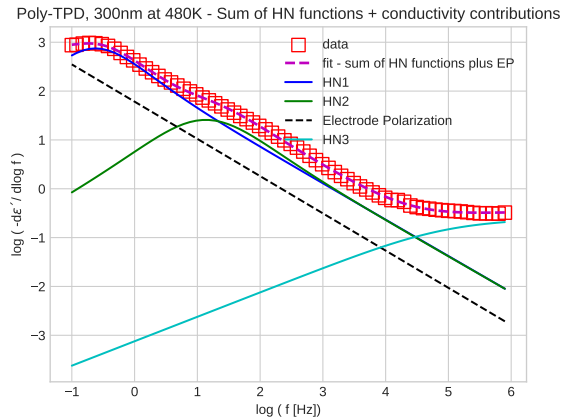
(a) Poly-TPD, 300nm, 450K



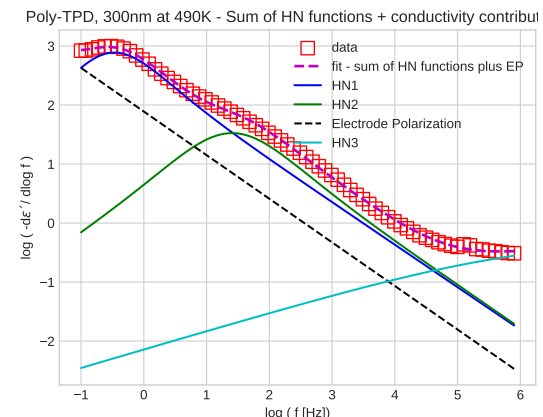
(b) Poly-TPD, 300nm, 460K



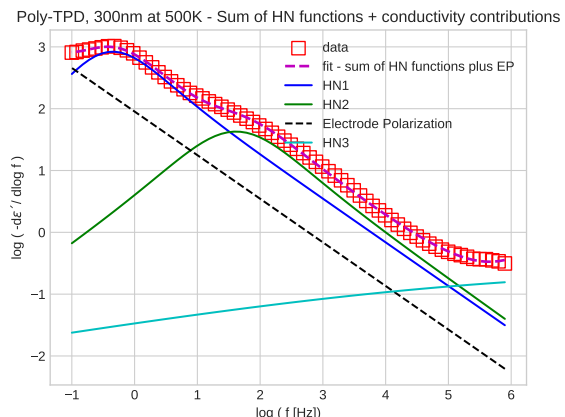
(a) Poly-TPD, 300nm, 470K



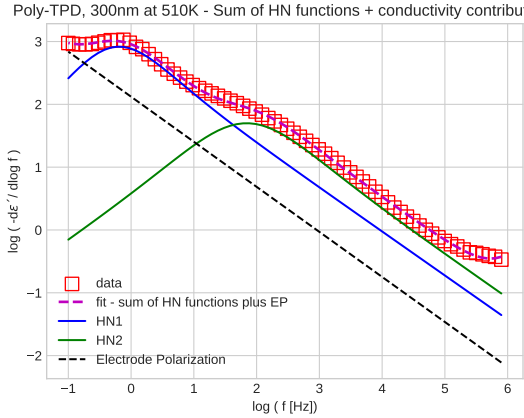
(b) Poly-TPD, 300nm, 480K



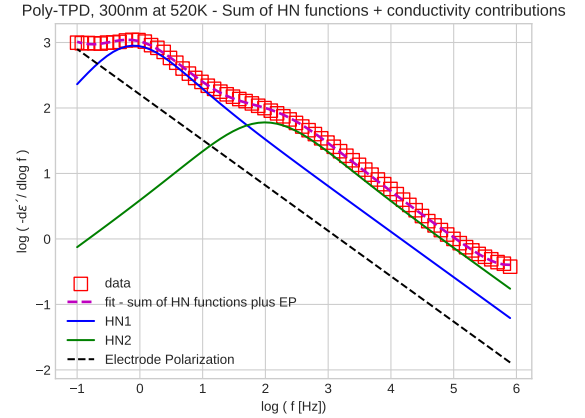
(a) Poly-TPD, 300nm, 490K



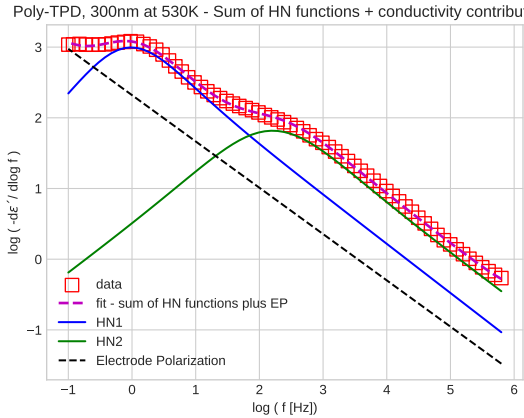
(b) Poly-TPD, 300nm, 500K



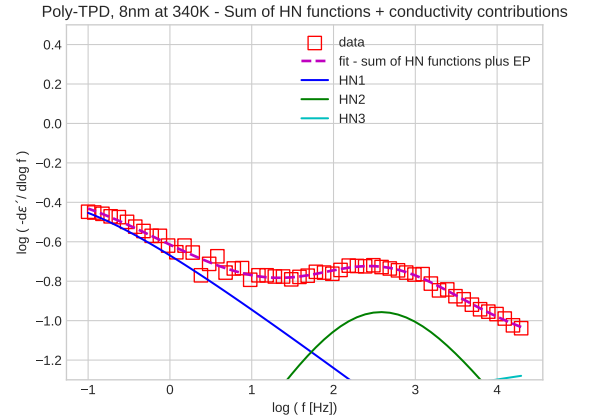
(a) Poly-TPD, 300nm, 510K



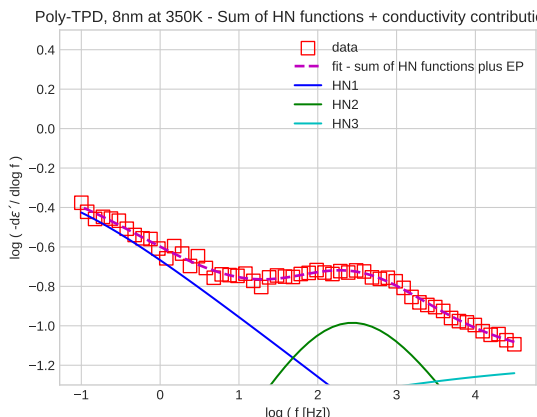
(b) Poly-TPD, 300nm, 520K



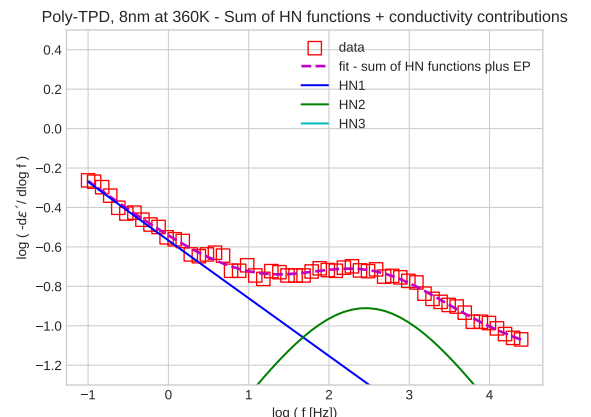
(a) Poly-TPD, 300nm, 530K



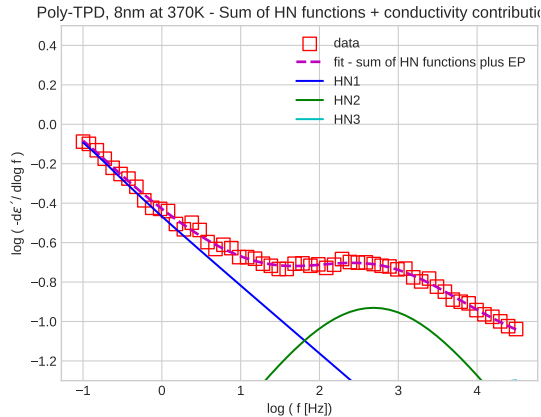
(b) Poly-TPD, 300nm, 340K



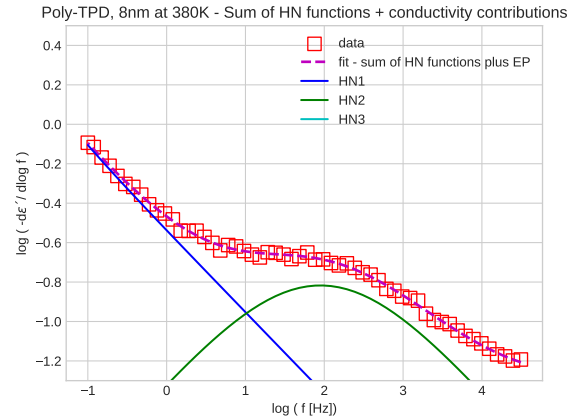
(a) Poly-TPD, 8nm, 350K



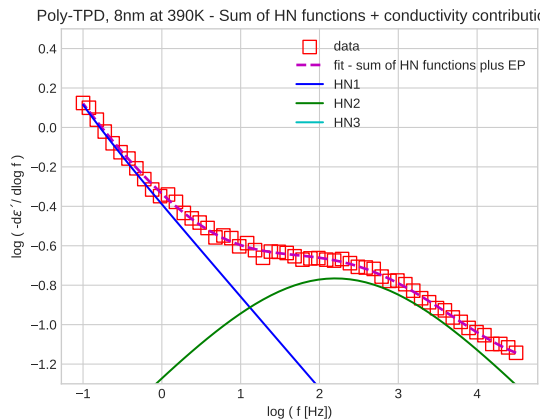
(b) Poly-TPD, 8nm, 360K



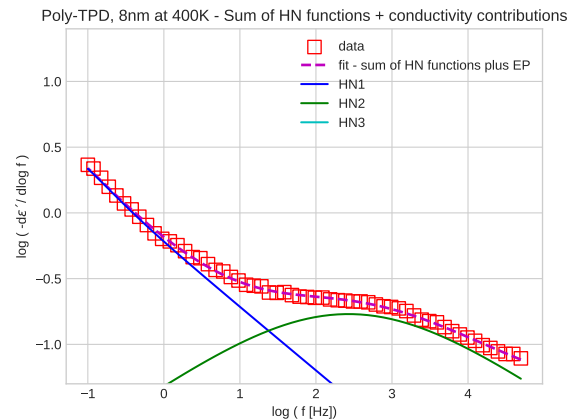
(a) Poly-TPD, 8nm, 370K



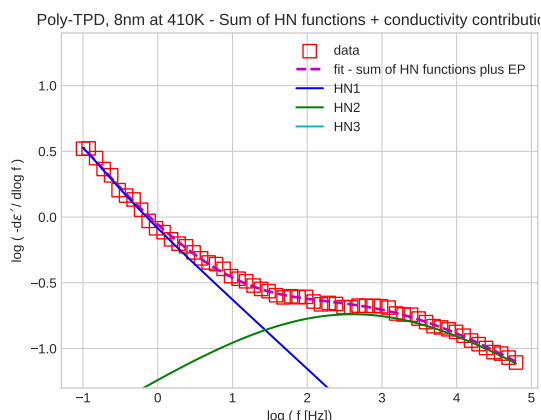
(b) Poly-TPD, 8nm, 380K



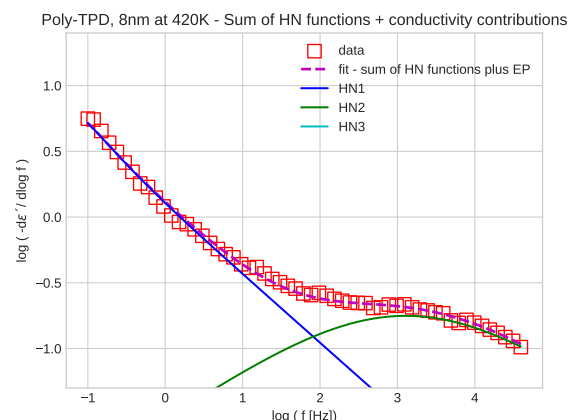
(a) Poly-TPD, 8nm, 390K



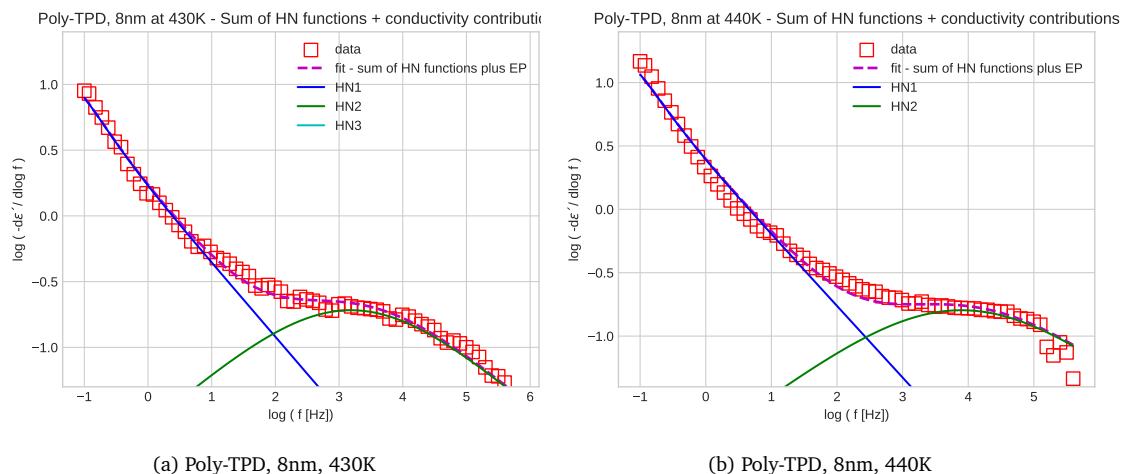
(b) Poly-TPD, 8nm, 400K



(a) Poly-TPD, 8nm, 410K



(b) Poly-TPD, 8nm, 420K



Appendix D

VFT/Arrhenius Fits

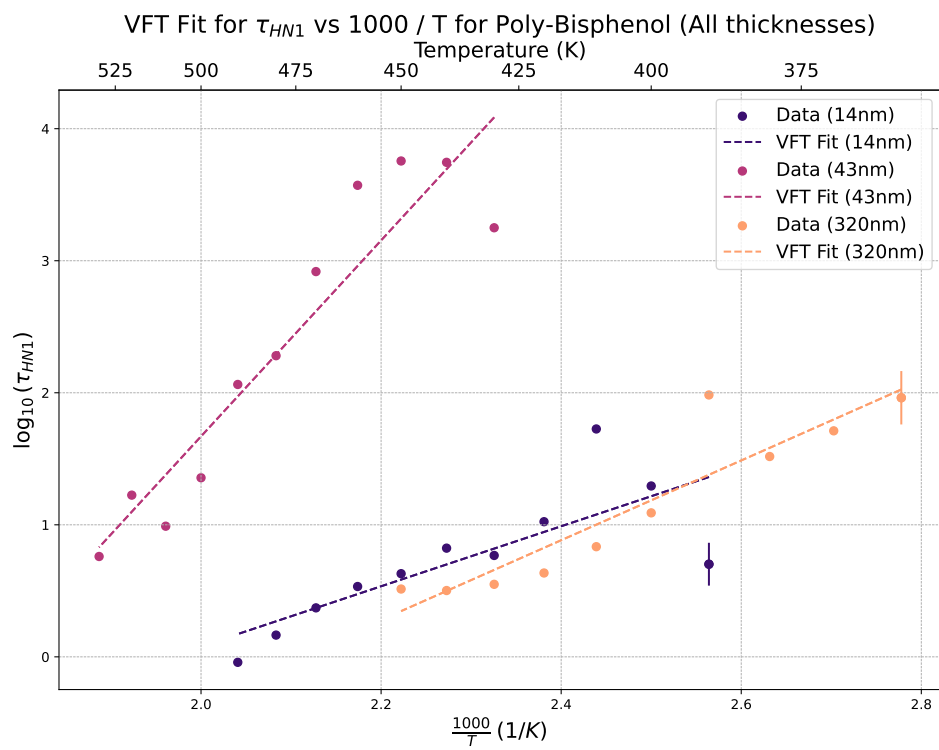


Figure D.1: Relaxation times of the first relaxation process (i.e. obtained from the HN1 function) occurring in Poly-Bisphenol at different thicknesses. This process appears to depend on thickness in a not-immediately-clear way. Further research may be needed for understanding this fully.

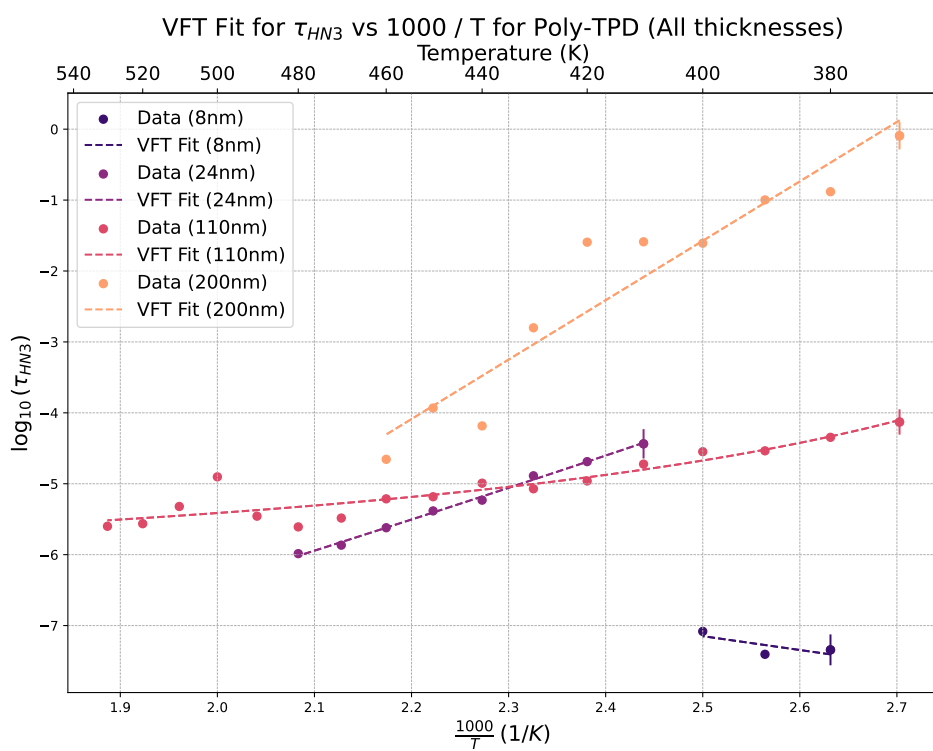


Figure D.2: Relaxation times of the third relaxation process (i.e. obtained from the HN3 function) occurring in Poly-TPD at different thicknesses. This relaxation process also looks to have a thickness dependence, although not as clear as the second relaxation process.

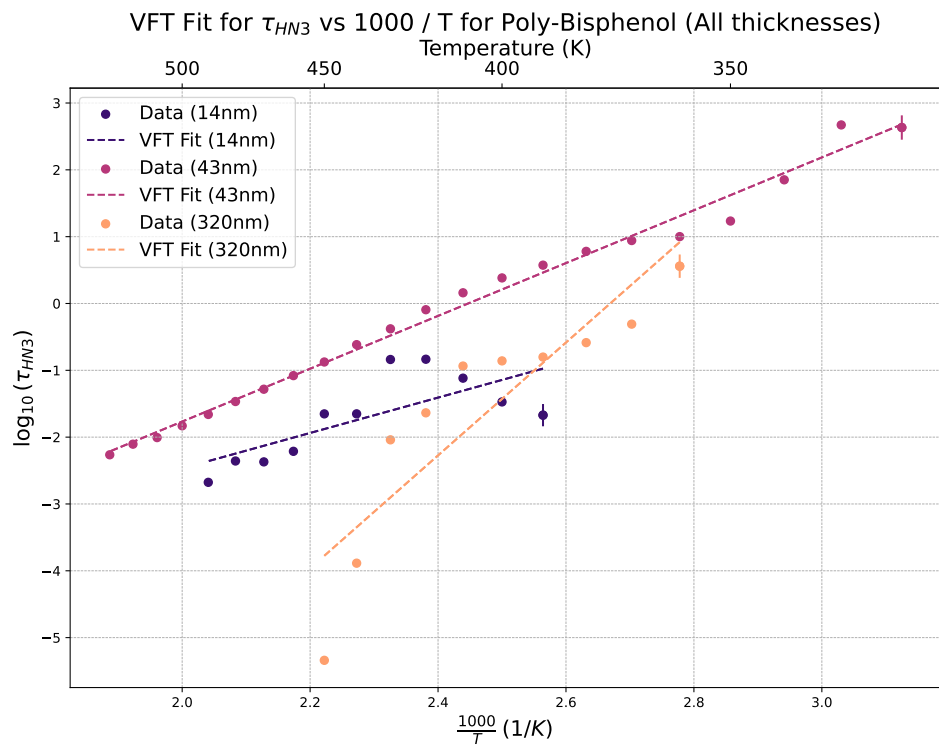


Figure D.3: Relaxation times of the third relaxation process (i.e. obtained from the HN3 function) occurring in Poly-Bisphenol at different thicknesses. It is still not clear whether the thickness correlation has a physical meaning or is simply due to e.g. errors in the fit.